IEEE Access
Multidisciplinary | Rapid Review | Open Access Journal

Received March 25, 2018, accepted April 19, 2018, date of publication April 26, 2018, date of current version May 16, 2018.

Digital Object Identifier 10.1109/ACCESS.2018.2830352

Longitudinally Uniform Transmission Lines With Frequency-Enabled Mode Conversion

DESONG WANG[1], (Student Member, IEEE), FAEZEH FESHARAKI[2], AND KE WU[1], (Fellow, IEEE)

[1]Poly-Grames Research Center, École Polytechnique de Montréal, Montreal, QC H3T 1J4, Canada
[2]Microsemi Corporation, Burnaby, BC V5A 4V7, Canada

Corresponding author: Desong Wang (desong.wang@polymtl.ca)

This work was supported in part by the Natural Sciences and Engineering Research Council of Canada Discovery Grant and in part by the NSERC Strategic Project.

ABSTRACT A class of longitudinally uniform transmission lines with low loss, low dispersion, and high-field confinement, called mode-selective transmission lines (MSTLs), has been proposed for ultra-broadband and ultra-fast electromagnetic signal guidance and processing. Their operation is mainly based on the concept of frequency-enabled mode selectivity. This paper presents our latest research results on this emerging MSTL, including its operating mechanism, propagation characteristics, higher-order modes, and transition design. Throughout the detailed discussion, two MSTL structures operating in distinct frequency ranges (DC to 60 GHz and DC to 500 GHz as showcased here) are considered. First of all, a comparative study among MSTLs and several conventional transmission lines is made, illustrating significant differences in structural features, wave guidance, field distributions, and frequency characteristics. Second, the phenomenon of mode selectivity occurred in MSTLs is examined by means of identified physical evidence (i.e., field distributions in connection with modal behavior) and theoretical foundation. It is verified that, with increasing frequency, the dominant modes of MSTLs are converted from a quasi-TEM microstrip mode to a quasi-TE_{10} waveguide mode over a certain frequency range. Following this thread, a more rigorous analysis is carried out by defining and formulating three characteristic frequencies based on the observed inherent physical dispersions, and the operating frequency ranges of MSTLs are thus divided into several distinct frequency regions associated with the frequency-related variable dominant mode. In addition, a general analysis of the attenuation characteristics of MSTLs and higher order modes in MSTLs is conducted. To facilitate practical measurements and to expedite the integrated applications of MSTLs, we propose a low-loss and ultra-broadband transition between MSTL and microstrip line, through which undesired higher order modes are effectively suppressed. The numerical and theoretical analyses of MSTLs are carried out with experimental verifications. At the end of this paper, different fabrication and measurement techniques for the two MSTLs of interest are briefly described.

INDEX TERMS Field distribution, high-order mode, mode-selective transmission line (MSTL), mode selectivity, propagation characteristic, quasi-TEM mode, quasi-TE_{10} mode, tapered transition.

I. INTRODUCTION

High-performance transmission lines and waveguides operating in the microwave, millimeter-wave, and terahertz (THz) frequency ranges, in support of ultra-broadband and ultra-fast signal generation, transmission, and processing, are indispensable building blocks for realizing and advancing cutting edge semiconductor and system technologies and applications for aerospace, defense, communications, sensing, data center, and various high-tech segments and markets. They are instrumental for current and future ICT-related hardware developments, such as chip-to-chip interconnects [1], [2], electro-optic modulators [3], [4], and detectors [5]. Over the past decades, significant efforts have been made for exploring high-performance transmission media, which are often concerned with incremental or limited improvements of conventional transmission lines and waveguides. Although the performance of conventional transmission media has improved continually thanks to structure and processing

innovations, they are still unable to meet the stringent requirements for high-quality ultra-broadband guided-wave signal propagation judging from propagation loss, frequency dispersion, and mode confinement. Non-TEM waveguides (such as rectangular waveguide (RWG) [6], [7], substrate integrated waveguide (SIW) [8], [9], and dielectric waveguide [10]–[12]) are subject to a strong frequency dispersion near the cutoff frequencies of guided modes. TEM-type lines (such as coplanar waveguide (CPW) [13], [14], microstrip line [15], [16], stripline [17], and coaxial line [18]) generally suffer from severe signal attenuations, especially at millimeter-wave and THz frequencies. In addition, higher-order modes are easily excited along these conventional transmission lines and waveguides [19]. These drawbacks (strong dispersion, high loss, and higher-order modes) fundamentally limit their applications in which low-loss, low-dispersion, ultra-broadband (e.g., DC to THz), or ultra-fast pulse (pico- or femto-second) propagation is often required. On the other hand, parallel-plate waveguides (PPWGs) [20], [21] and metal wires [22], [23] have been demonstrated to potentially guide an ultra-broadband electromagnetic wave with low loss and low dispersion. However, a significant diffraction loss, especially for a long propagation length, deteriorates the performance of PPWGs. Poor mode confinement and difficulty of mode excitation are few hurdles to the applications of metal wires.

A new concept of mode-selective transmission line (MSTL) has recently been proposed in [24]–[26]. This kind of transmission medium is capable of guiding an ultra-broadband (e.g., DC to THz) signal with low loss and low dispersion [24], [25]. Preliminary research results indicate that MSTL operates in a variable dominant mode, which can be converted from a quasi-TEM microstrip mode to a quasi-TE_{10} waveguide mode as frequency increases. A prevailing assumption or perception about a transmission medium with a given cross section has been that a mode conversion (or called mode coupling, mode transition, or mode transformation) can only occur when there is a geometrical discontinuity or perturbation along the propagation direction of the guided wave [27]–[29]. In [30], a mode conversion from a TEM-like mode to a plasmon-like mode has been observed in a PPWG when frequency goes up. Similarly, a phenomenon of frequency-enabled mode conversion appears in the longitudinally uniform MSTLs proposed in [24]–[26]. These facts reveal that a mode conversion may occur in a transmission medium without being subjected to any longitudinal irregularities.

This mode conversion makes MSTL versatile, benefitting from combined advantages of the two modes. The quasi-TEM microstrip mode gets rid of the cutoff frequency and dispersive behavior over a low-frequency range, whereas the quasi-TE_{10} waveguide mode allows a relatively low signal attenuation and reduced dispersion over a high-frequency range. In this paper, the specific phenomenon of frequency-enabled mode conversion is called "mode selectivity" to highlight its essential difference as opposed to the classical perception. The operation of MSTL, in fact, is mainly based on the mode selectivity. Field distributions for various field components of the dominant mode of a typical MSTL were examined in [31], becoming a first-hand physical evidence of the mode selectivity. In this work, we begin with reviewing our previous research on MSTL (referring to [24]–[26] and [31]) and then present our latest research findings through the analysis and demonstration of two practical MSTL examples (one is proposed in this paper, and the other MSTL was presented in our previous work [24], [25]). The main contributions of this work are listed as follows: (1) MSTLs are compared in detail to conventional transmission media; (2) Theoretical foundations of mode selectivity are provided; (3) Characteristic frequencies are defined and formulated to quantify the mode selectivity; (4) Propagation characteristics of MSTLs are investigated based on the defined frequency regions; (5) Higher-order modes in MSTLs are treated for the first time, and the effective suppression of these undesired modes is demonstrated; (6) Field transformation in the tapered transition reported in [25] is examined; (7) Finally, the low-frequency (DC to 60 GHz) MSTL is experimentally verified to further examine the MSTL technique.

This paper is organized as follows. In Section II, MSTLs are compared to conventional transmission media in terms of structural features, wave guidance, field distributions, and frequency characteristics. Section III is concerned with the mode selectivity in MSTLs, which is verified by both physical evidence and theoretical foundation. It is followed by a more rigorous analysis of the mode selectivity in Section IV. In this section, characteristic frequencies are defined, and several frequency regions are specified accordingly. In Section V, a general analysis of signal attenuation and a brief discussion of higher-order modes in MSTLs are conducted. A low-loss and ultra-broadband microstrip-to-MSTL transition is presented in Section VI, and different fabrication and measurement techniques for the two MSTLs are briefly described. Finally, this work is concluded in Section VII.

II. MSTL STRUCTURE

A typical topology of MSTL is shown in Fig. 1, which may be regarded as a geometrical superposition of microstrip line, coplanar waveguide (CPW), substrate integrated waveguide, *etc* [32]. The geometrical parameters are also labeled in the figure. A conducting strip of width w is centered between two identical side conducting planes of thickness t and conductivity σ, constructing two identical slits of width s and offset distance m. They are printed on a thin conductor-backed dielectric substrate of thickness h, relative permittivity ε_r, and loss tangent $\tan\delta$. The side conducting planes are connected to the bottom conducting plane through two lateral conducting sidewalls of separation d. A close look of Fig. 1 shows that MSTL is symmetric about the yoz plane and uniform along the propagation direction of guided wave (z-axis in Fig. 1(a)); it is longitudinally uniform. On the other hand, MSTL is

TABLE 1. Dimensions of both MSTL I and MSTL II.

	h	d	m	w	s	t	ε_r	tanδ	σ
MSTL I	0.254 mm	3 mm	0.45 mm	0.65 mm	0.25 mm	18 μm	10.2 (ceramic PTFE)	0.0023	5.8×10^7 S/m (copper)
MSTL II	50 μm	600 μm	89 μm	140 μm	38 μm	2 μm	4.27 (crystal quartz)	0.0002	6.1×10^7 S/m (silver)

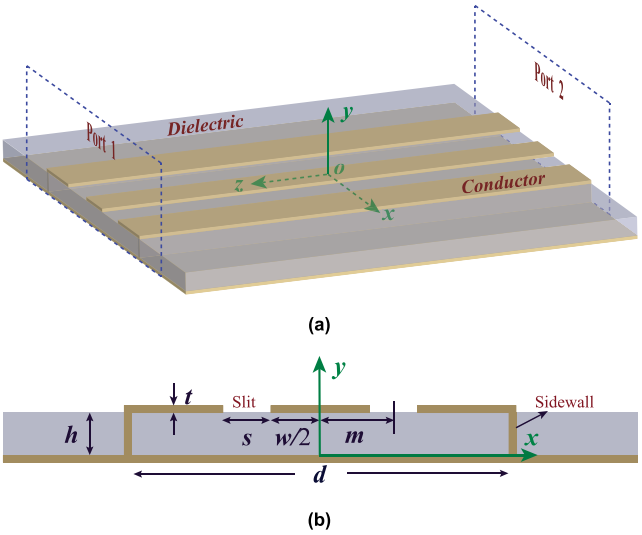

FIGURE 1. Typical topology of MSTL. (a) Perspective view. (b) Cross-sectional view.

asymmetric and inhomogeneous with respect to the y-axis because of the hybrid air (for $y > h + t$) and dielectric regions (for $0 < y < h$). For this reason, the two-conductor MSTL cannot support the guidance of a pure TEM wave, resulting from an impossible phase-matching condition at the dielectric-air interface. As briefly mentioned earlier, MSTL can be viewed as a composite transmission line [33] from which we can see the footprints of different well-known transmission media, such as microstrip line, slotline, conductor-backed CPW (CBCPW), dielectric-filled RWG (i.e., SIW), half-mode SIW (or called half-width microstrip line), *etc*. This feature may cause higher-order modes in MSTL, which will be discussed in more detail in Section V. Given the similarity of structures, we focus on comparing MSTL in this section with the conventional CBCPW and RWG in terms of structural features, wave guidance, field distributions, and frequency characteristics.

Two practical MSTL examples operating in distinct frequency ranges are considered for a comprehensive study. One operates from DC to 60 GHz, and the other operates from DC to 500 GHz (proposed in [24]), which are called MSTL I and MSTL II for simplicity, respectively. Their dimensions are listed in Table 1. For the according discussions of these MSTLs later, it is necessary to introduce three characteristic frequencies, f_{ms1}, f_{ms}, and f_{ms2} ($f_{ms1} < f_{ms} < f_{ms2}$), ahead of time, which will be defined in Section IV to quantify the mode selectivity in MSTL. When frequency f is below f_{ms1} ($f < f_{ms1}$), the dominant mode of MSTL is the quasi-TEM microstrip mode. In contrast, when f is above f_{ms2} ($f > f_{ms2}$), the dominant mode is converted to the quasi-TE$_{10}$ waveguide mode. At a frequency in between (e.g., f_{ms}), the dominant mode is a kind of hybrid "transition" mode. In the following discussions, we will focus on the results and phenomena at these characteristic frequencies because of their applicability for different MSTLs.

Full-wave analyses are carried out using a commercially available finite-element method software package (ANSYS Electronics Desktop 2017) [34], [35]. Given that the dominant mode of MSTL would change with frequency, wave ports supporting various propagation modes are used to feed the uniform MSTL, as labeled in Fig. 1(a). For simplicity of analysis, the lateral sidewalls are modeled by conducting solid walls if no otherwise specified. Surface roughness of conductors, skin effect, and material dispersion are not considered in the simulation models.

A. COMPARISON WITH CBCPW

As we can see from Fig. 1, the typical MSTL structure itself resembles a conventional CBCPW with bilateral sidewalls [36]–[38] (also called channelized CPW [39] or grounded CPW [40]). There are, however, many important differences between MSTL and CBCPW, such as dominant modes, frequency characteristics, and excitation methods. The most significant and substantial difference lies in their dominant modes. The dominant mode of MSTL can be converted from a quasi-TEM microstrip mode to a quasi-TE$_{10}$ waveguide mode with increasing frequency (i.e., mode selectivity), whereas the dominant quasi-TEM CPW mode of CBCPW remains unchanged over its frequency range of operation. The mode selectivity contributes to unique properties of MSTL, such as low loss, low dispersion, and ultra-broad frequency range of operation [24]–[26], which are rather challenging to obtain for a conventional CBCPW. Another difference is the excitation method. For a CBCPW, the feed point is generally located directly on the central strip [41]. In contrast, it is necessary for MSTL to feed the whole cross-sectional area with the aid of specially designed transitions, which will be discussed in Section VI-A.

In this subsection, the dominant mode of MSTL at frequencies f below f_{ms1} ($f < f_{ms1}$) is discussed and compared to that of CBCPW. A sketch of the cross-sectional electric and magnetic field lines for the dominant mode of MSTL when $f < f_{ms1}$ is given in Fig. 2(a). For comparison, the field lines for the standard CPW mode in a CPW and for the standard microstrip mode in a microstrip line are plotted in Figs. 2(b) and (c). The electric and magnetic field lines in MSTL are roughly divided into two parts, Part I (gray lines) and Part II (color lines)

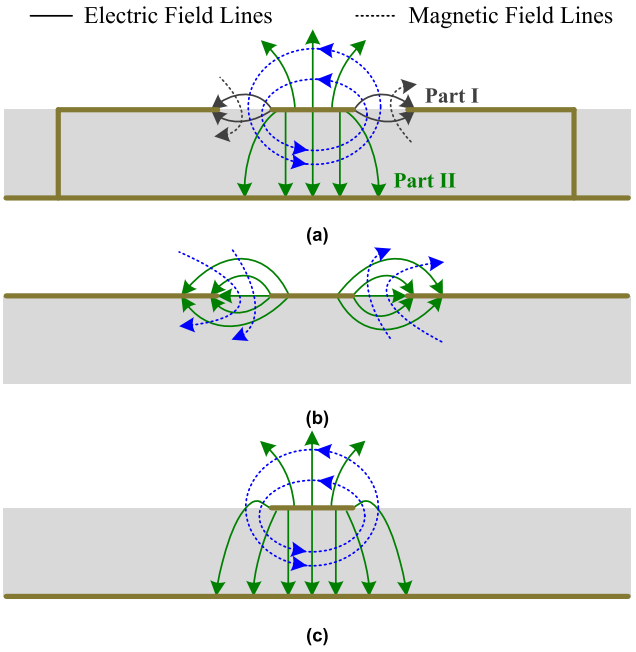

FIGURE 2. Cross-sectional electric and magnetic field lines in (a) MSTL when frequency f is below f_{ms1} (or CBCPW), (b) CPW, and in (c) microstrip line.

(as labeled in Fig. 2(a)), to simplify the following analysis. Part I is similar to the field lines in the CPW (see Fig. 2(b)), which is primarily determined by the central strip together with the side conducting planes of MSTL. Part II is similar to the field lines in the microstrip line (see Fig. 2(c)), which is primarily determined by the central strip together with the bottom conducting plane of MSTL. The dominant mode of MSTL at low frequencies ($f < f_{ms1}$), in fact, becomes analogous to that of a CPW or that of a microstrip line depending on the dimensions. For example, increasing the slit width s or decreasing the substrate thickness h of MSTL (Fig. 1) while keeping other parameters fixed can weaken Part I but strengthen Part II. That is, the dominant mode of MSTL tends to resemble that of a conventional microstrip line (i.e., quasi-TEM microstrip mode). On the other hand, as the slit width s decreases or the substrate thickness h increases, the dominant mode of MSTL tends to resemble that of a conventional CPW (i.e., quasi-TEM CPW mode). In fact, the field lines in the conventional CBCPW are similar to those in MSTL in this case [36]. A similar phenomenon of the mode also exists in CBCPW [36], [42]. The CPW mode is generally preferable to the microstrip mode in CBCPW by strengthening Part I and weakening part II. On the contrary, the microstrip mode is preferable in MSTL when $f < f_{ms1}$. The main reason is that the effective permittivity for the microstrip mode is in a level close to that for the high-frequency waveguide mode in MSTL, thus maintaining a relatively stable effective permittivity (i.e., low frequency dispersion) over the frequency range of interest [26]. For the two MSTL examples considered in this work, the dielectric substrates used are extremely thin ($h < (w + 2s)/4$) so that their dominant modes are the quasi-TEM microstrip mode when $f < f_{ms1}$. In one word, MSTL performs similarly to a microstrip line rather than a CBCPW or a CPW when frequency f is below f_{ms1}. When frequency continues to increase, the dominant mode of MSTL will be converted to a quasi-TE_{10} waveguide mode, becoming similar to the dominant mode of RWG, as discussed later.

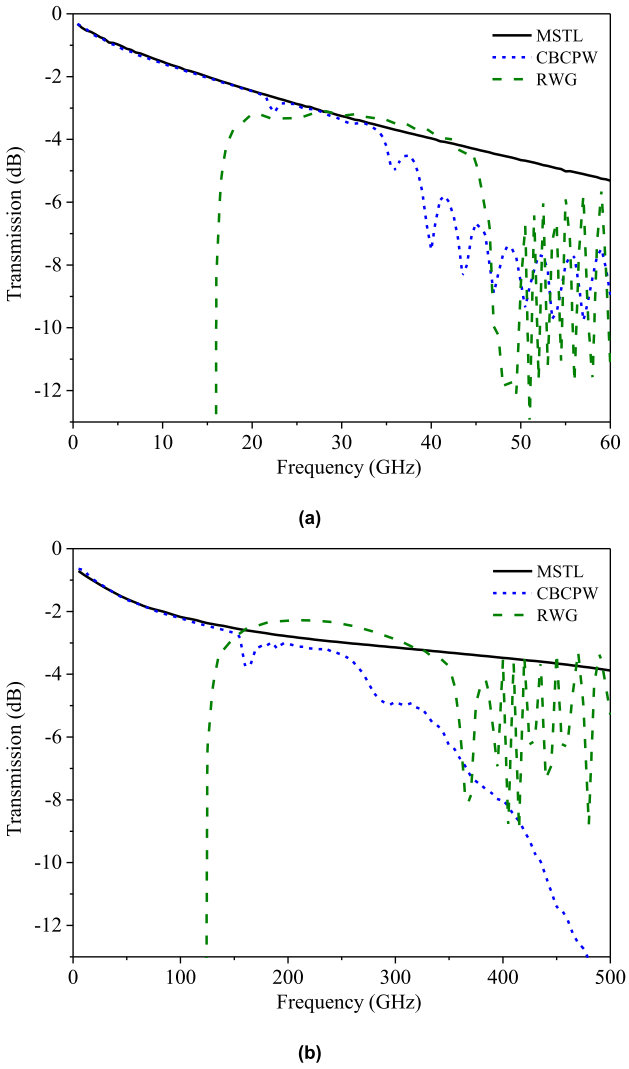

FIGURE 3. Comparison between transmission responses of MSTLs and CBCPW and RWG counterparts. (a) MSTL I. (b) MSTL II.

To demonstrate the difference of performance between MSTL and CBCPW, simulated transmission responses of the two MSTL examples (see Table 1) and their CBCPW counterparts are all plotted in Fig. 3 for comparison. To emulate practical situations and to facilitate measurement interfaces, we use the microstrip-to-MSTL and microstrip-to-CBCPW feed lines into the corresponding simulation models. The overall lengths of MSTL I and MSTL II including transitions (see Section VI-A) are 76 and 14 mm, respectively. The CBCPW counterparts have the same shapes and sizes but different excitation methods [43]. From Fig. 3, the

transmission curves of both MSTL I and MSTL II are smooth over the whole frequency ranges. In contrast, many sharp dips appear at high frequencies in the curves of CBCPW counterparts. This is because the resonances and leakage of laterally spreading fields cause these sharp dips, thus severely degrading the performance of CBCPWs [43]–[45].

B. COMPARISON WITH RWG

In addition to CBCPW, the typical MSTL structure also resembles a dielectric-filled RWG with two additional slits etched symmetrically in the top conducting plane. This feature contributes to the guided wave performance of MSTL at frequencies f above f_{ms2} ($f > f_{ms2}$). That is, MSTL performs similarly to a dielectric-filled RWG when $f > f_{ms2}$. In this case, the dominant mode of MSTL tends to resemble the dominant TE_{10} mode of RWG; in fact, it is a quasi-TE_{10} waveguide mode in MSTL because of the additional slits [2]. It should be noted that MSTL is a two-conductor transmission medium that its dominant mode does not possess a cutoff frequency. This high-frequency waveguide mode in MSTL is, in fact, converted from the low-frequency microstrip mode as frequency increases. A sketch of the electric and magnetic field lines for the dominant quasi-TE_{10} waveguide mode of MSTL at high frequencies ($f > f_{ms2}$) is described in Fig. 4(a), compared to those for the dominant TE_{10} mode of the dielectric-filled RWG in Fig. 4(b). It can be observed that the field lines in MSTL in this case are similar to those in RWG except for a slight difference around the two slits. This indicates that MSTL should have the guided wave performance similar to that of a dielectric-filled RWG when $f > f_{ms2}$.

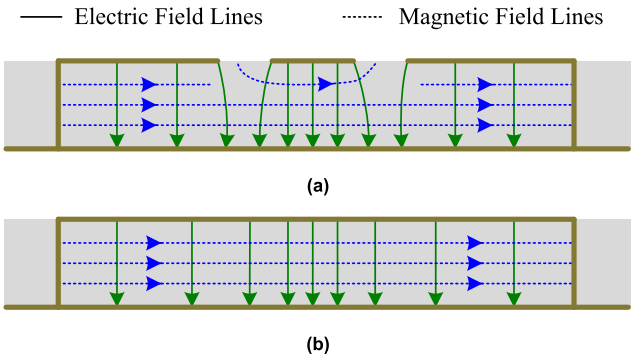

FIGURE 4. Cross-sectional electric and magnetic field lines in (a) MSTL when frequency f is above f_{ms2} and in (b) RWG.

Similarly, the simulated transmission curves of the dielectric-filled RWG counterparts (i.e., SIWs) of both MSTL I and MSTL II are obtained and plotted in Fig. 3 for comparison. The microstrip-to-SIW transitions presented in [46] are used in the simulation models to emulate practical situations including measurement purposes. As can be seen, the RWG counterparts operate in narrow frequency ranges, resulting from the low-frequency cutoff and excitation of higher-order modes (e.g., TE_{30} mode) [47]. These MSTLs and their RWG counterparts show similar transmission responses over the common frequency ranges. The difference between the power losses, as a result of the additional slits in MSTLs, is negligible when considering practical influence factors such as conductor surface roughness and skin depth. This will be demonstrated by comparing the measured transmission responses of MSTL I and its RWG counterpart in Section VI (see Fig. 20).

III. MODE SELECTIVITY

Now consider the phenomenon of mode selectivity occurring in MSTL in this section. As we know, the change of the dominant mode of MSTL is reflected directly in the change of electric and magnetic field distributions. Therefore, field distributions for the dominant mode of MSTL are examined thoroughly, which turn out to be an important physical evidence of mode selectivity. The orthogonality relations between the hybrid TM and TE modes in MSTL are then presented, providing a theoretical foundation of mode selectivity.

A. PHYSICAL EVIDENCE

To better understand the mechanism of physics, let us begin with the consideration of a simple microstrip line that supports the propagation of quasi-TEM mode. The use of terminology "quasi-TEM mode" is directly related to the existence of a longitudinal magnetic field component, which is generally negligible compared to its dominant TEM field components. The occurrence of such a longitudinal component is caused by the cross-sectional non-uniformity or discontinuity along the microstrip line. Generally, this longitudinal field may become more and more pronounced as frequency increases. This can be observed as dispersion becomes stronger. Still, the longitudinal field is relatively weak in most cases as long as the geometrical conditions of relevance favor the guidance of a quasi-TEM mode. Of course, this phenomenon may create a favorable condition for high-order mode leakage and also for high-order mode generations if a longitudinal discontinuity is introduced. On the other hand, one may also imagine that there is a special uniform geometry that can be designed and used to favor and strengthen this longitudinal magnetic field component such that it cannot be negligible beyond certain frequency point. Therefore, the resulting mode would be characterized by three field components, which in fact form a quasi-TE mode in this case. This would create a new mode conversion or simply MSTL, which spells out the fundamental physical mechanism. The schematic diagram of this kind of mode conversion is depicted in Fig. 5. As can be seen, the magnitude of the longitudinal magnetic field component $|H_z|$ for the dominant mode of MSTL continues to increase as frequency increases. As a result, $|H_z|$ of MSTL is becoming higher than that of microstrip (quasi-TEM mode) at around f_{ms1} and then approaching that of RWG (TE_{10} mode) at around f_{ms2}. This change of the important field component H_z results in the mode conversion between the quasi-TEM mode and the quasi-TE_{10} mode in MSTL. This phenomenon

TABLE 2. Electric field distributions in MSTL, microstrip line, and RWG.

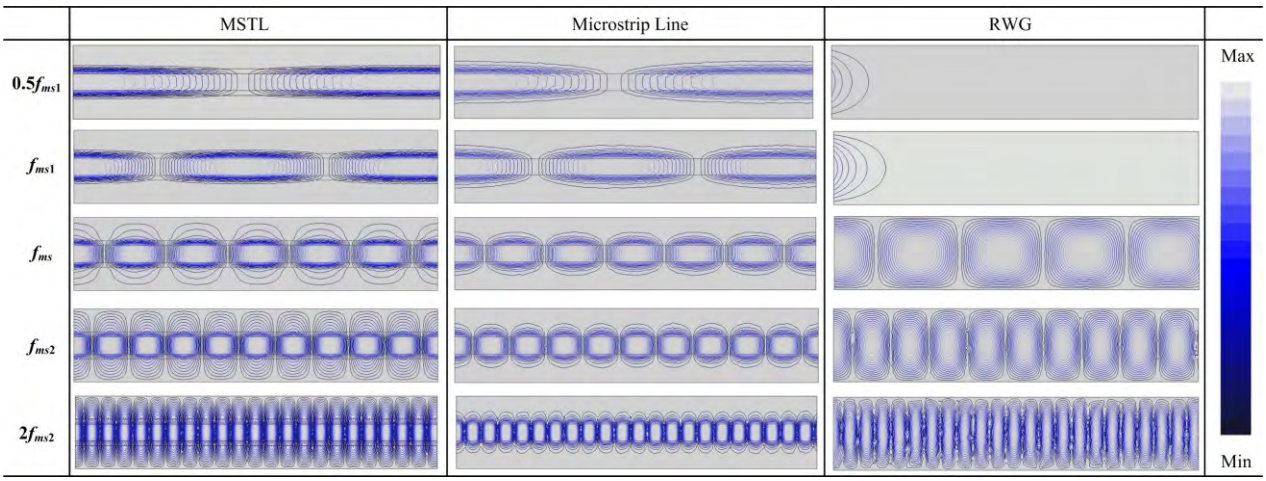

TABLE 3. Magnetic field distributions in MSTL, microstrip line, and RWG.

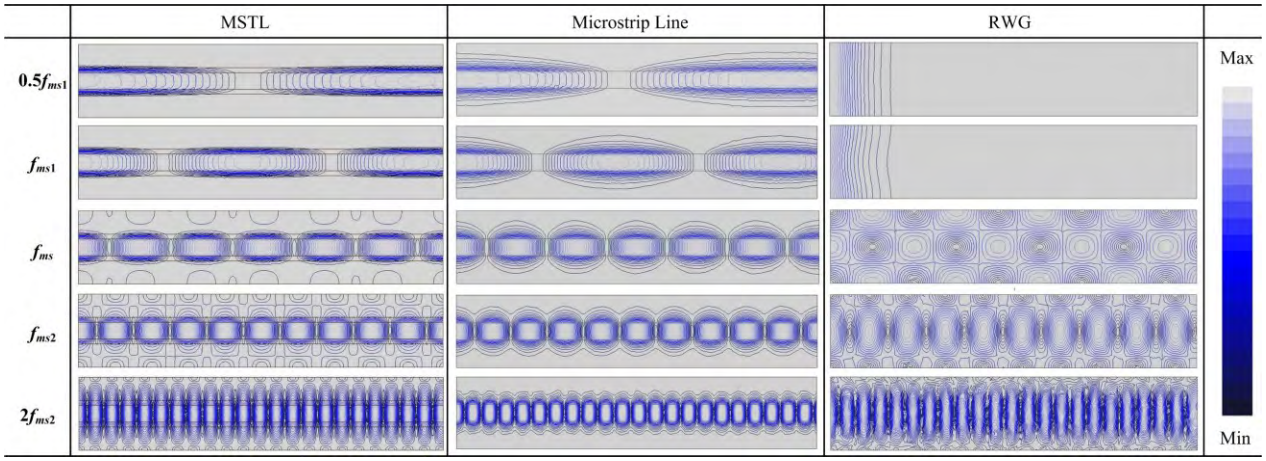

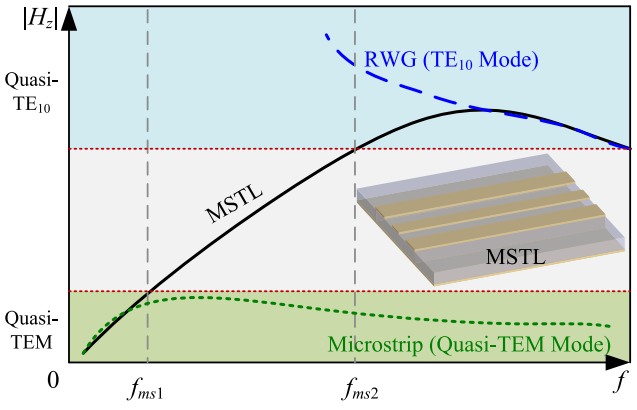

FIGURE 5. Schematic diagram of mode conversion in MSTL on the basis of the frequency-related variable longitudinal magnetic field component H_z.

will be further demonstrated and discussed by examining the practical field distributions in MSTL as follows.

For MSTL II, the field distribution curves for all the field components of the dominant mode have been extracted and discussed in [31], showing that the fields in MSTL smoothly change with frequency. The electric and magnetic field lines for the variable dominant mode of MSTL are also compared to those in conventional transmission media in the preceding section. In the present subsection, we further investigate and look into the field distributions in MSTL, which are compared to those in the RWG and microstrip counterparts at specific frequency points.

In different MSTLs (e.g., MSTL I and MSTL II), field distributions at corresponding frequencies are almost the same, as a result of the same operating mechanism (i.e., mode selectivity). Electric and magnetic field distributions for the dominant modes of MSTLs at $0.5f_{ms1}$, f_{ms1}, f_{ms}, f_{ms2}, and $2f_{ms2}$ are considered here, as listed in Table 2 and Table 3. It should be emphasized that these frequency points are specified to simplify the unified analyses for different MSTLs. In fact, one can choose arbitrary frequencies; however, we suggest considering the frequencies across the different frequency regions (to be specified in Section IV) for a clear comparison. Similarly, the field distributions for the dominant modes of the microstrip and RWG counterparts are also

sketched and listed in Table 2 and Table 3 for comparison. The field distributions for the dominant mode of MSTL at different frequencies are different, as expected. To be specific, the fields in MSTL at $0.5f_{ms1}$ and f_{ms1} are bounded around the central strip, which are analogous to those in the microstrip counterpart. The dominant TE_{10} mode of RWG is below cutoff at these frequencies. At f_{ms2} and $2f_{ms2}$, partial fields spread to the side parts of MSTL, thus tending to resemble those in the RWG counterpart. This change of the field distributions in MSTL indicates the change of the dominant mode of MSTL. That is, the dominant mode of MSTL at a low frequency (e.g., $0.5f_{ms1}$ or f_{ms1}) is analogous to the dominant mode of the microstrip counterpart; that is a quasi-TEM microstrip mode. As frequency increases to a relatively high frequency (e.g., f_{ms2} or $2f_{ms2}$), the dominant mode of MSTL tends to be resemble the dominant mode of RWG; that is a quasi-TE_{10} waveguide mode. At a frequency in between (e.g., f_{ms}), the dominant mode of MSTL is a hybrid "transition" mode. The change of the dominant mode of MSTL is indeed describable by the mode selectivity, which occurs smoothly as frequency increases [31]. The reason is that the boundary conditions "seen" by the dominant propagating mode of MSTL change gradually with increasing frequency. Specifically, the boundary conditions for the dominant mode of MSTL at a low frequency (e.g., $0.5f_{ms1}$ or f_{ms1}) are almost the same as those for the dominant mode of the microstrip counterpart. As frequency increases to a higher frequency (e.g., f_{ms2} or $2f_{ms2}$), the side conducting planes together with the sidewalls (see Fig. 1) have a much-pronounced effect. Hence, the boundary conditions for the dominant mode of MSTL in this case become analogous to those for the dominant mode of the RWG counterpart.

In addition to the electric and magnetic field distributions in MSTL, it is worthwhile to further examine the major field components of the dominant mode of MSTL. As we know from [31], E_y, H_x, and H_z are the major field components. Their magnitude curves along the x-axis (at $y = h/2$) in Fig. 1 at $0.5f_{ms1}$, f_{ms1}, f_{ms}, f_{ms2}, and $2f_{ms2}$ are extracted using the HFSS field calculator [35], as plotted in Fig. 6. The field magnitude curves are normalized to the maximum magnitudes of the electric field component and the magnetic field component. The normalized field magnitude curves of the microstrip counterpart at $0.5f_{ms1}$ and the RWG counterpart at $2f_{ms2}$ are also plotted in Fig. 6 for comparison. For MSTL, the major field components (E_y, H_x, and H_z) have a noticeable change in their distribution shape and magnitude as frequency increases gradually. It is found that the $|E_y|$, $|H_x|$, and $|H_z|$ curves of MSTL at $0.5f_{ms1}$ are similar to those of the microstrip counterpart at $0.5f_{ms1}$. As frequency continues to increase from $0.5f_{ms1}$ to $2f_{ms2}$, both the left and right parts of all the field curves of MSTL rise remarkably. As a result, the field curves of MSTL are becoming similar to those of the RWG counterpart, especially at $2f_{ms2}$. For the microstrip and RWG counterparts, on the other hand, the field magnitude curves have a slight change with increasing frequency [19], [31], [48]. This reveals the conversion of the dominant mode

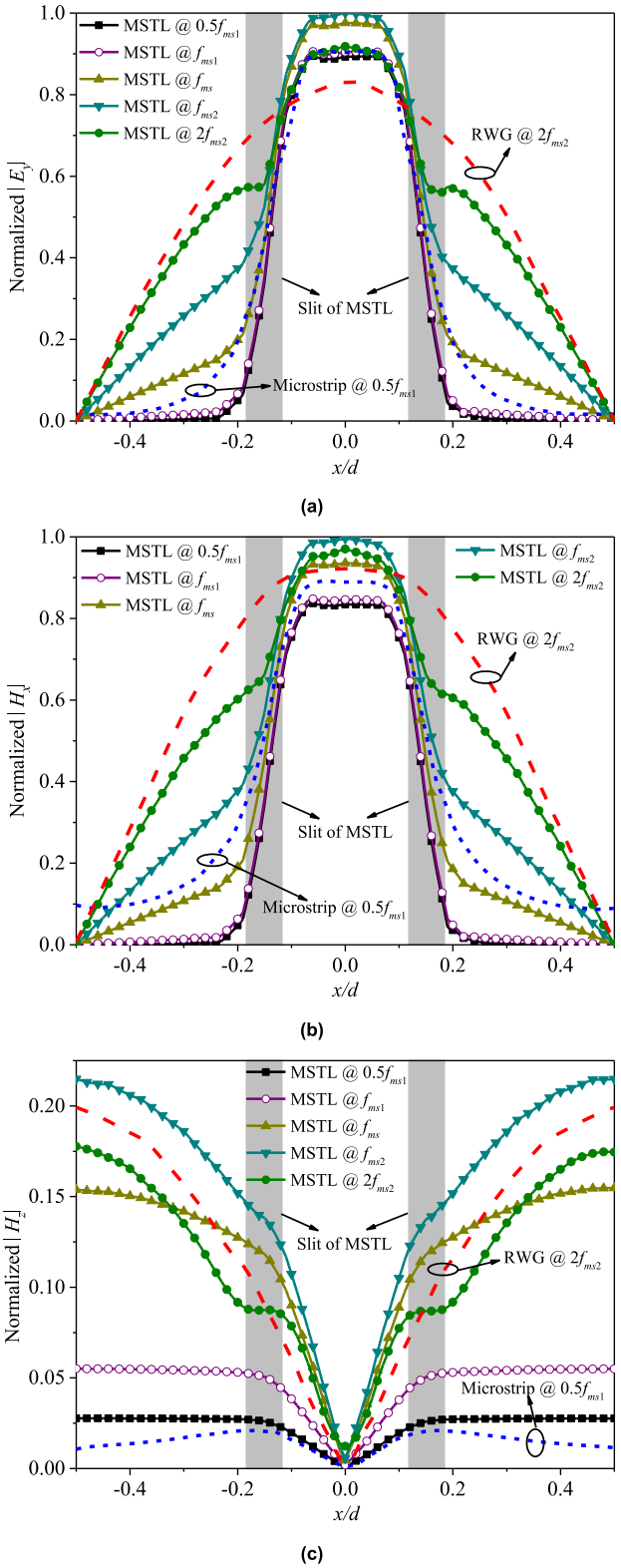

FIGURE 6. Normalized field magnitude curves of MSTL and the microstrip and RWG counterparts along the x-axis in Fig. 1. (a) E_y field component. (b) H_x field component. (c) H_z field component.

of MSTL. Given the changes of other field components E_x, H_y, and E_z of MSTL (both $|E_x|$ and $|H_y|$ decrease with frequency, and $|E_z| \approx 0$) [31], we can conclude that the

dominant mode of MSTL is changed smoothly from a quasi-TEM microstrip mode to a quasi-TE_{10} waveguide mode with increasing frequency. The examination, comparison, and analyses of the field distributions in MSTL and its counterparts provide a substantial physics-based proof of the mode selectivity in MSTL.

B. THEORETICAL FOUNDATION

MSTL is asymmetric and inhomogeneous with respect to the y-axis because of the different (or hybrid) dielectric regions (see Fig. 1), as described in Section II. For this reason, MSTL cannot support a pure dominant TEM mode or a pure dominant TE (or TM) waveguide mode. As described in Chapter 3 in [11] and [49], the fields in a composite transmission system (e.g., MSTL) can be expanded into a complete set of known modes. These known modes do not individually satisfy the boundary conditions of the composite system and hence couple to each other. In fact, the exact fields in MSTL constitute a hybrid TM-TE wave, as in a microstrip line or a CPW. The TE^y and TM^y hybrid modes with respect to the y direction are considered to simplify the study of the air-dielectric interface in the y direction. Due to the unbounded y and z directions (see Fig. 1), the hybrid TE^y and TM^y modes have complex propagation factors in the y and z directions, k_y and k_z. For a laterally shielded top-open transmission line like MSTL, the hybrid TE^y and TM^y modes satisfy the following orthogonality relations [50]:

$$P^{i,j}_{m,n} = \int_{-d/2}^{d/2} \left[\vec{e}^{\,i}_m(x) \times \left(\vec{h}^{\,j}_n\right)^*(x)\right] \cdot \hat{y} \cdot dx = \begin{cases} 1, & \text{if } m = n \text{ and } i = j \\ 0, & \text{if } m \neq n \text{ and } i \neq j \\ C, & \text{if } m = n \text{ and } i \neq j \end{cases} \quad (1)$$

where $\vec{e}^{\,i}_m$ and $\vec{h}^{\,j}_n$ are the transverse vector modal functions with respect to the y direction. The indexes m and n represent the orders of modes, and i and j are used to distinguish between TE and TM polarizations with respect to the y direction. From [50], we know that the parameter C in (1) is nonzero as long as k_z is not a pure real number. These types of modes exist in MSTL because of the evanescent and leaky waves in the z propagation direction. This fact indicates that complex hybrid modes with the same orders (i.e., $m = n$) but different polarizations (i.e., $i \neq j$) are nonorthogonal. That is, a significant coupling effect can occur along the transverse direction (y-axis) between the TE^y and TM^y hybrid modes.

In MSTL, the TE^y modes could be coupled to the same-order TM^y modes with increasing frequency. The strength of coupling would decrease as the order ($m = n$) of the coupled modes increases [50]. This is consistent with the change of the field distributions in MSTL. As detailed in [31], when frequency increases, the magnitudes of the field components E_y, H_x, and H_z increase, and the magnitude of E_z is still close to zero, whereas the magnitudes of E_x and H_y decrease gradually. In addition to the change in magnitudes, there is an obvious change in shapes of the distribution curves of the field components [31]. As a result of the significant coupling effect, the change of field distributions in MSTL is reflected in the change of the dominant mode as a whole, i.e., mode selectivity. We emphasize that the dominant quasi-TEM mode at low frequencies and the dominant quasi-TE_{10} mode at high frequencies are confirmed by rigorously examining the field distributions at different frequencies. The above analysis rovides a theoretical foundation of the phenomenon of mode selectivity in MSTL.

IV. CHARACTERISTIC FREQUENCIES

In the preceding section, it has been verified that the dominant mode of MSTL appears in two dissimilar forms (quasi-TEM and quasi-TE_{10} modes), supported by the mode selectivity. A more rigorous analysis of the mode selectivity is carried out in this section. The characteristic frequencies, f_{ms1}, f_{ms2}, and f_{ms}, are first defined and formulated. With these frequency points, the whole frequency range of MSTL can then be divided into several frequency regions, Region I, Region II (Region II-A and Region II-B), and Region III, associated with the variable dominant mode.

To quantify the mode selectivity in MSTL, it is necessary to treat and then model the quasi-TEM and quasi-TE_{10} modes separately. For the individual quasi-TEM microstrip mode, the sidewalls (see Fig. 1) are placed close to the slits. This leads to that the "appearance" (cutoff) frequency of the waveguide mode increases and is thus completely outside the frequency ranges of interest. It should be noted that the sidewalls should not be too close to the slits, which may result in undesirable interference with the central bound fields of the quasi-TEM mode [51]. For the individual quasi-TE_{10} waveguide mode, all the top conductors (see Fig. 1) are set at the same voltage level. In fact, this realizes a dielectric-filled RWG with two symmetric slits etched in the top conducting plane, called two-slit RWG for short [52], which has a dominant quasi-TE_{10} mode [2]. In this way, the individual quasi-TEM and quasi-TE_{10} modes in MSTL can be analyzed numerically. The individual quasi-TE_{10} mode is also analyzed using empirical equations, which will be given later. The individual quasi-TEM mode is considerably similar to the dominant mode of a conventional microstrip line. Therefore, it is convenient to determine the propagation characteristics of the individual quasi-TEM mode by using the well-known equations about those of a microstrip line presented in [19] and [48], as well as considering the effect of the side conducting planes [53]. It is therefore not repeated in this work.

Both MSTL I and MSTL II continue to be considered as examples for the following discussions. With the simulation models of MSTL and of the individual quasi-TEM and quasi-TE_{10} modes, their phase constants β are obtained and plotted in Fig. 7, normalized to the free-space phase constant k_0. It is found that the curves of the normalized phase constants of both MSTL I and MSTL II are continuous and flat all over the frequency ranges, indicating low frequency dispersion [24]–[26].

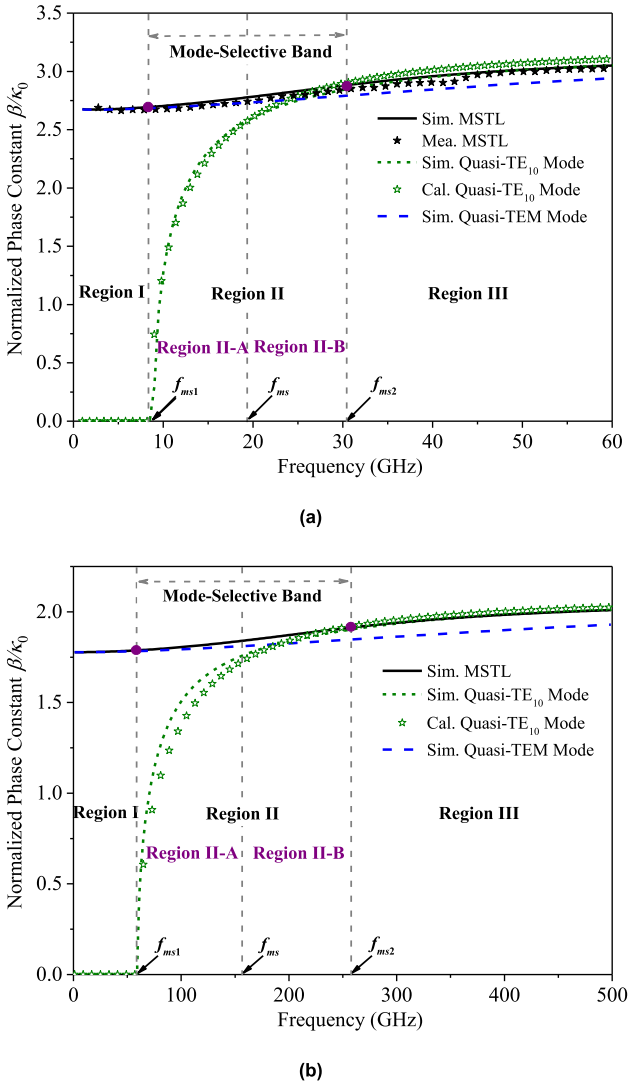

FIGURE 7. Comparison between normalized phase constants of MSTLs, individual quasi-TEM modes, and individual quasi-TE_{10} modes. (a) MSTL I. (b) MSTL II.

In Figs. 7(a) and (b), three critical frequency points, f_{ms1}, f_{ms2}, and f_{ms}, and several frequency regions, Region I, Region II (Region II-A and Region II-B), and Region III, are clearly labeled, which will be defined and discussed in more detail.

A. APPEARANCE FREQUENCY OF QUASI-TE_{10} MODE f_{ms1}

The first characteristic frequency f_{ms1} is defined as the "appearance" frequency of the quasi-TE_{10} mode in MSTL, meaning the quasi-TE_{10} mode begins to appear at this frequency. This indicates that the dominant mode of MSTL is the quasi-TEM mode when frequency f is below f_{ms1} ($f < f_{ms1}$). As seen from Fig. 7(a) or Fig. 7(b), f_{ms1} corresponds to the high-frequency end of the overlapping curve of MSTL and the individual quasi-TEM mode. This characteristic frequency is also the cutoff frequency of the individual quasi-TE_{10} mode. Its value can be determined with the help of the proposed models of the individual modes. It is also possible to determine its value directly by calculating the cutoff frequency of the individual quasi-TE_{10} mode. As described before, the individual quasi-TE_{10} mode can be modeled by a two-slit RWG. Many methods can be used to analyze slitted RWGs, such as transverse resonance analysis [2], [54], and numerical modeling [52]. In this work, we propose a simple but rigorous method to analyze the two-slit RWG (i.e., the individual quasi-TE_{10} mode). It is based on an assumption that the two-slit RWG evolves from a single-slit RWG, finally traced back to a dielectric-filled RWG. The method is detailed in Appendix. On the basis of the proposed method, an empirical equation is given to calculate the characteristic frequency f_{ms1} as

$$f_{ms1} = \frac{2}{M\sqrt{\mu_0\varepsilon_0(\varepsilon_r + 0.34)}} - \frac{1}{2d\sqrt{\mu_0\varepsilon_0\varepsilon_r}} \tag{2}$$

where μ_0 and ε_0 are the permeability and permittivity in free space, and ε_r represents the relative permittivity of the dielectric substrate used. The variable M is formulated as

$$M = \begin{cases} 2d + 3.69m + 2h - 2.25s & \text{for } s \geq 0.7h \\ 2d + 3.69m + \frac{h^2}{s} - h & \text{for } s < 0.7h \end{cases} \tag{3}$$

where all the parameters have been defined in Section II. With the given dimensions (see Table 1), the characteristic frequencies f_{ms1} for MSTL I and MSTL II are calculated to be 8.6 and 59 GHz, respectively, in agreement with the simulated 8.5 and 58 GHz. The phase constant of the individual quasi-TE_{10} mode is also formulated (see (12) in Appendix) and plotted in Fig. 7. It can be observed that the calculated phase constants of the individual quasi-TE_{10} modes agree well with the simulated ones over the whole frequency ranges.

B. MAXIMUM-COUPLING FREQUENCY f_{ms2}

The second characteristic frequency f_{ms2} is defined as the maximum-coupling frequency at which the maximum mode coupling between the quasi-TEM and quasi-TE_{10} modes takes place. This indicates that the dominant mode of MSTL is converted to the quasi-TE_{10} mode when frequency f is above f_{ms2} ($f > f_{ms2}$). With reference to Fig. 7(a) or Fig. 7(b), f_{ms2} corresponds to the low-frequency end of the overlapping curve of MSTL and the individual quasi-TE_{10} mode. This phenomenon is consistent with the coupled-mode theory [32], [55]. With a curve-fitting method [56], [57], an empirical equation is proposed to calculate this characteristic frequency as

$$f_{ms2} = \frac{1}{[1.34\,(d-h) - 1.55\,(w-2s)]\sqrt{\mu_0\varepsilon_0(\varepsilon_r - 1.23)}}. \tag{4}$$

The accuracy of (4) is verified through taking MSTL II as an example. As detailed in Appendix, comparison results indicate that, within the design region of MSTL defined in [26], (4) can be used to accurately predict the characteristic frequency f_{ms2} with a calculation error below 5%. For MSTL I and MSTL II, the characteristic frequency f_{ms2} calculated by (4) are 29.1 and 261 GHz, respectively, in agreement with the

simulated 30.5 and 260 GHz. The frequency ranges of both MSTL I (DC to 60 GHz) and MSTL II (DC to 500 GHz) considered in this work are from DC to around $2f_{ms2}$, limited basically by the fabrication and measurement techniques, which will be described in Section VI.

C. MODE-SELECTIVE FREQUENCY f_{ms}

As described above, the dominant mode of MSTL is the quasi-TEM mode when $f < f_{ms1}$ and the quasi-TE_{10} mode when $f > f_{ms2}$, respectively. Within the frequency range from f_{ms1} to f_{ms2} ($f_{ms1} \leq f \leq f_{ms2}$), the dominant mode of MSTL experiences a gradual change from the quasi-TEM mode to the quasi-TE_{10} mode with increasing frequency. This change is evident from the field distributions [31]. This frequency range is therefore defined as the mode-selective band, as labeled in Fig. 7. The dominant mode of MSTL within this frequency band is a hybrid "transition" mode varying with frequency. A characteristic frequency termed the mode-selective frequency f_{ms} is defined to bound the mode-selective band in this paper. Due to the gradual change of the field distributions, the frequency point f_{ms} should be located around the center of the mode-selective band, thereby expressed as

$$f_{ms} \approx \frac{f_{ms1} + f_{ms2}}{2}. \tag{5}$$

The calculated f_{ms} for MSTL I and MSTL II are 18.85 and 160 GHz, respectively. The simulated and calculated values of all the characteristic frequencies are listed in Table 4. We can conclude that, within the mode-selective band ($f_{ms1} \leq f \leq f_{ms2}$), the quasi-TEM mode prevails when frequency f is below f_{ms} ($f < f_{ms}$), whereas the quasi-TE_{10} mode prevails when f is above f_{ms} ($f > f_{ms}$).

TABLE 4. Simulated and calculated characteristic frequencies (unit: GHz).

		f_{ms1}	f_{ms}	f_{ms2}	Mode-Selective Band
MSTL I (DC-60 GHz)	Sim.	8.5	19.5	30.5	22 (8.5-30.5)
	Cal.	8.6	18.85	29.1	20.5 (8.6-29.1)
MSTL II (DC-500 GHz)	Sim.	58	159	260	202 (58-260)
	Cal.	59	160	261	202 (59-261)

With these characteristic frequencies, the whole frequency range of MSTL can be divided into several frequency regions including Region I, Region II (Region II-A and Region II-B), and Region III, as labeled in Figs. 7(a) and (b). In Region I ($f < f_{ms1}$), the dominant mode of MSTL is the quasi-TEM mode and its frequency characteristics are remarkably analogous to those of a microstrip line. In Region II ($f_{ms1} \leq f \leq f_{ms2}$), i.e., mode-selective band, the dominant mode is a hybrid "transition" mode performing as a quasi-TEM mode in Region II-A ($f_{ms1} \leq f < f_{ms}$) and as a quasi-TE_{10} mode in Region II-B ($f_{ms} < f \leq f_{ms2}$). In Region III ($f > f_{ms2}$), the dominant propagating mode of MSTL is the quasi-TE_{10} mode; its frequency characteristics closely resemble those of a dielectric-filled RWG. These conclusions are tabulated in Table 5. In one word, the mode selectivity enables the longitudinally uniform MSTL to operate in a dominant mode varying with frequency. It can be rigorously treated using these defined characteristic frequencies.

TABLE 5. Frequency regions and corresponding dominant modes.

Region I	Region II		Region III
$f < f_{ms1}$	$f_{ms1} \leq f \leq f_{ms2}$		$f > f_{ms2}$
	Region II-A	Region II-B	
	$f_{ms1} \leq f < f_{ms}$	$f_{ms} < f \leq f_{ms2}$	
Quasi-TEM Mode	Hybrid Mode		Quasi-TE_{10} Mode
	Quasi-TEM Mode	Quasi-TE_{10} Mode	

V. ATTENUATION CHARACTERISTICS AND HIGHER-ORDER MODES

The phase constants of both MSTL I and MSTL II have been examined when defining the characteristic frequencies in the preceding section (see Fig. 7). It implies that the phase characteristics of MSTL can be determined by treating the individual modes. In this section, we focus on the attenuation characteristics of both MSTL I and MSTL II. We will also briefly discuss the higher-order modes in these MSTLs. As can be seen from Fig. 1, MSTL is a sort of composite transmission line from which we can see the footprints of different well-known transmission media. This feature may lead to higher-order modes in MSTL. In this section, the first hree higher-order modes are examined and briefly discussed, which could be generated in both MSTL I and MSTL II over the frequency ranges of interest, i.e., DC to $2f_{ms2}$.

A. ATTENUATION CHARACTERISTICS

In general, the signal attenuation in a transmission line or waveguide is caused by dielectric loss and conductor loss [19]. The total attenuation constant α can be expressed as $\alpha = \alpha_d + \alpha_c$ where α_d and α_c represent the attenuation due to dielectric loss and the attenuation due to conductor loss, respectively. Fig. 8 shows the curves of $\alpha_d$and α_c of both MSTL I and MSTL II, compared to those of the individual quasi-TEM and quasi-TE_{10} modes separately modeled in Section IV. It is seen that the attenuations, α_d and α_c, of these MSTLs are almost the same as those of the quasi-TEM modes when frequency f is below f_{ms} ($f < f_{ms}$) and as those of the quasi-TE_{10} modes when $f > f_{ms}$, respectively. This phenomenon is consistent with the previous comparison results among their phase constants (see Fig. 7). It implies that the attenuation characteristic of MSTL can be determined by separately treating the individual modes.

The simulated attenuation constants (α_d and α_c) of both MSTL I and MSTL II are compared to those of the RWG and microstrip counterparts for a further presentation of the attenuation characteristics of MSTL, as plotted in Fig. 9. The difference between the attenuation constants α_d of both MSTL I and MSTL II and their microstrip counterparts are small, especially when $f < f_{ms}$. The difference among the total attenuation constants α of these transmission media is

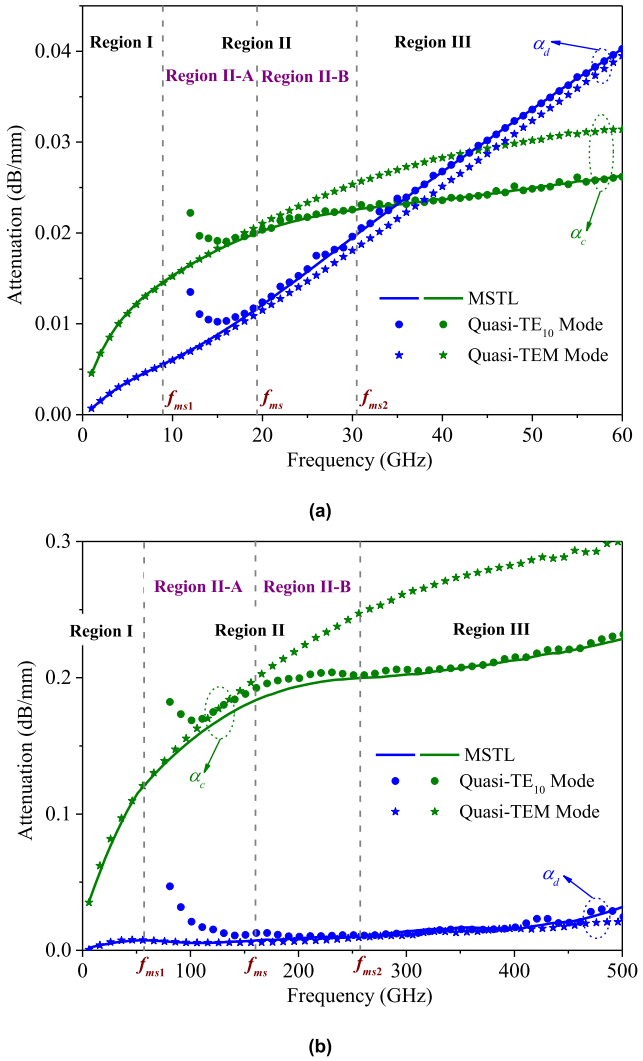

FIGURE 8. Comparison between attenuation constants of MSTLs, individual quasi-TEM modes, and individual quasi-TE$_{10}$ modes. (a) MSTL I. (b) MSTL II.

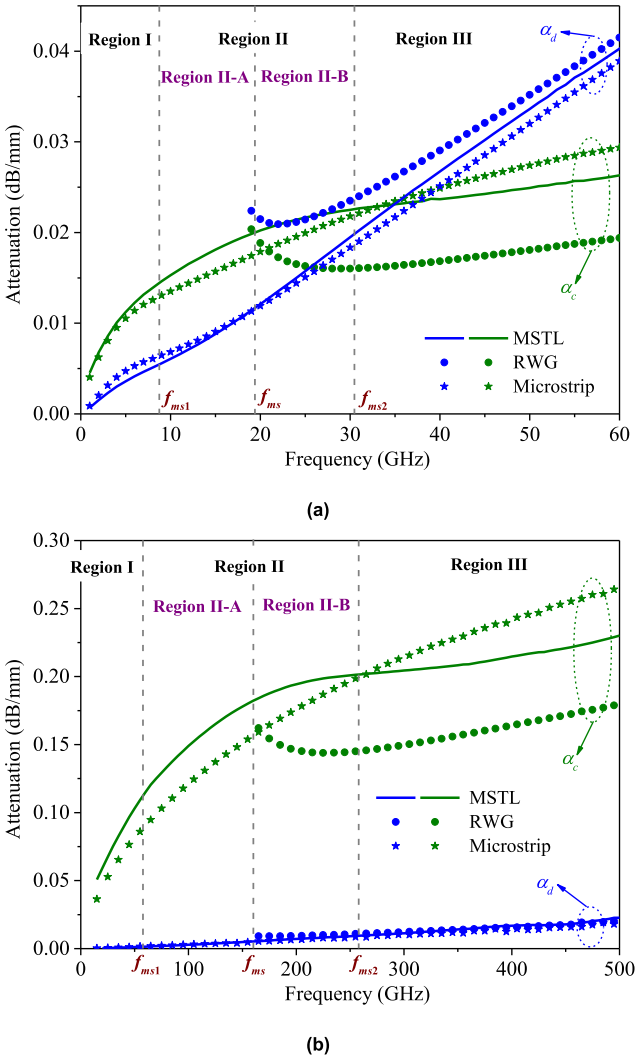

FIGURE 9. Comparison between attenuation constants of MSTLs and RWG and microstrip counterparts. (a) MSTL I. (b) MSTL II.

mainly caused by the difference among the attenuations due to conductor loss α_c. As can be seen, α_c of the MSTLs are slightly higher than those of the microstrip counterparts in both Region I and Region II because of the effects of the side conducting planes [53]. However, α_c of the MSTLs are becoming smaller in Region III in which the dominant modes of the MSTLs have been converted to the quasi-TE$_{10}$ waveguide mode. It is reasonable that α_c of the MSTLs are higher than those of the RWG counterparts in Region III, resulting from the two slits of the MSTLs. A closer examination of Fig. 9 shows that the α_c curves of the MSTLs are parallel to those of the RWG counterparts in Region III. This implies that we could consider an impact factor into the formula of the conductor loss of RWG (e.g., 3.96 of [19]) to determine the conductor loss of MSTL when $f > f_{ms2}$ (Region III).

From Figs. 8 and 9, one can find that the attenuation due to dielectric loss α_d of MSTL II is considerably small when compared to the attenuation due to conductor loss α_c. This is attributed to the used dielectric material (crystal quartz) with an extremely low loss tangent of $\tan\delta = 0.0002$ [58]. Here the effects of the loss tangent $\tan\delta$ of dielectric material and the conductivity σ of conductor material on the attenuation constants of MSTL II are investigated, compared to those of the RWG and microstrip counterparts. As depicted in Fig. 10, both the conductivity and loss tangent have effects on the attenuations as expected. This suggests that a proper material selection can help to reduce the power loss of MSTL to some extent. Despite these effects, the relationship between the attenuations of MSTL II and its RWG and microstrip counterparts remains the same, as described before.

With reference to Figs. 8, 9, and 10, the attenuations of both MSTL I and MSTL II increase gradually with frequency. We can also find that the difference among the attenuations of the transmission media is mainly caused by the different attenuations due to conductor loss α_c. To maintain a relatively low and stable attenuation over the frequency range of operation, it is necessary to further reduce the attenuations, in particular at higher frequencies. In addition to the material

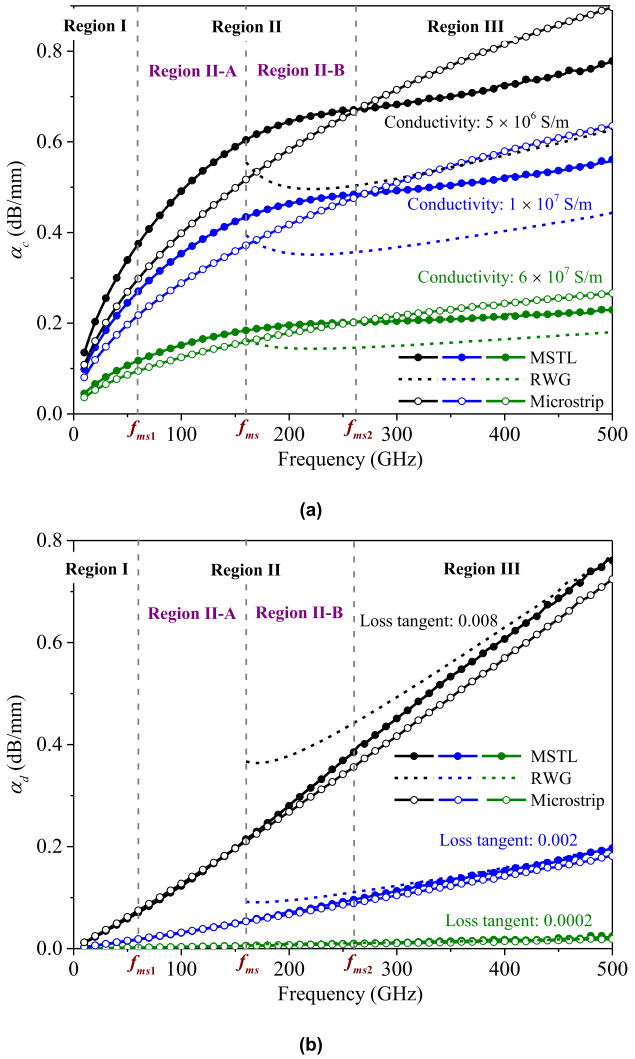

FIGURE 10. Comparison between attenuation constants of MSTL II and its RWG and microstrip counterparts. (a) Attenuation due to conductor loss α_c. (b) Attenuation due to dielectric loss α_d.

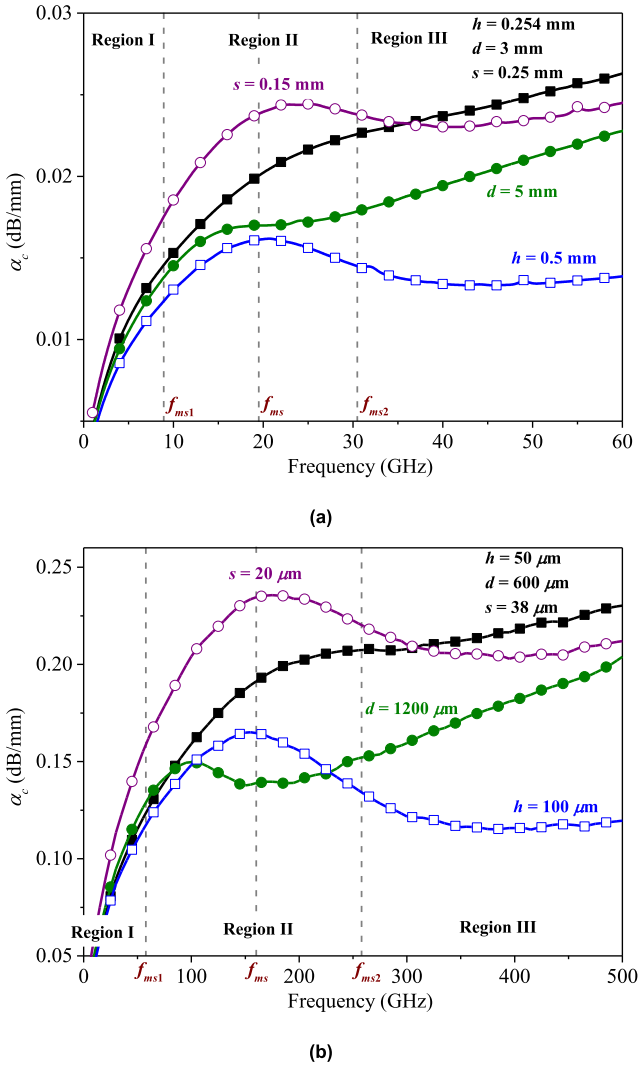

FIGURE 11. Effects of parameters on the attenuation due to conductor loss of (a) MSTL I and (b) MSTL II.

selection, we further study the effects of major geometrical parameters of the MSTLs, including substrate thickness h, sidewall span d, and slit width s (labeled in Fig. 1), on the attenuation due to conductor loss α_c. As plotted in Fig. 11, the increase of d or h can reduce the attenuation constant α_c when $f > f_{ms}$, which is mainly because of the decreased power density [19]. They have little effects on the attenuation constant α_c when $f < f_{ms}$. In contrast, s has adverse effects on the attenuation constant α_c in Region II and Region III. The different effects of these parameters on the attenuation constant α_c in different frequency regions are due to the variable dominant modes of the MSTLs. The change in values of these parameters also affects the characteristic frequencies and then the frequency regions.

B. HIGHER-ORDER MODES

The longitudinally uniform MSTL may support several higher-order modes. Phase constant curves plotted in Fig. 12 indicate that three higher-order modes could be generated in both MSTL I and MSTL II in the frequency ranges of interest (i.e., DC to $2f_{ms2}$). Their electric field distributions are sketched in Fig. 13. A close inspection of Figs. 13(a) and (b) shows that the electric fields of both the first and second higher-order modes concentrate mainly around the side parts of MSTL. The side parts, which consist of the side conducting planes, lateral sidewalls, and bottom conducting plane, can be considered as two symmetric half-width microstrips [59] (also called half-mode SIWs [57]). Referring to [2] and [59], we know that the first and second higher-order modes are even and odd EH_1 modes (also called the quasi-$TE_{0.5,0}$ modes [57]), respectively. It is seen from Fig. 13(c) that the electric fields of the third higher-order mode concentrate mainly around the central part of MSTL. The central part, which consists of the central strip and the bottom conducting plane, can be considered as a microstrip line. This implies that the third higher-order mode of MSTL is the first higher-order mode of the central microstrip line, i.e., EH_1 mode. Note that for these higher-order modes, partial fields around the silts

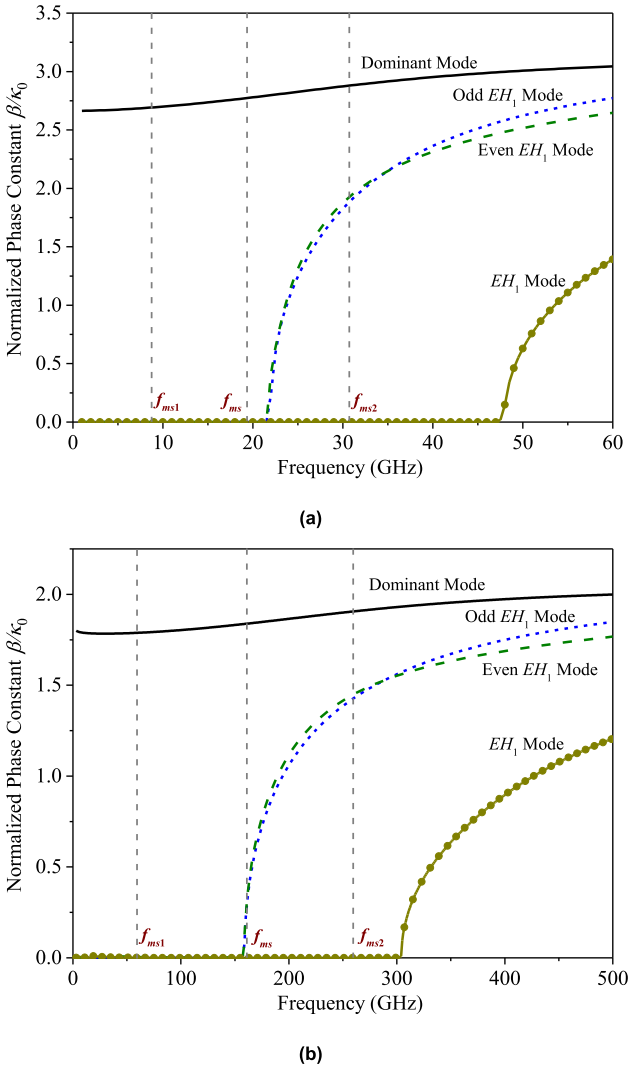

FIGURE 12. Normalized phase constants of various modes in (a) MSTL I and (b) MSTL II.

as observed from Fig. 13 contribute the portion of slotline modes; however, they are relatively weak when compared to the EH_1 mode.

We have compared the field distributions and phase characteristics of these higher-order modes in both MSTL I and MSTL II with those of the corresponding modes in the separate side parts and central part. The comparison results indicate that the corresponding modes show almost the same properties. This fact indicates that we can separately treat the higher-order modes by analyzing the separate side parts and central part of MSTL. This analysis can refer to the reported methods [57], [59]. It is not repeated here for simplicity. Other modes, such as slotline modes, surface wave modes, and other higher-order modes, could be generated in MSTL [25], [26] when frequency continues to increase, or any discontinuities are introduced. In practical applications, these undesired modes need to be suppressed or eliminated. To this end, a tapered transition is designed, able to effectively suppress the undesired modes over the frequency range of interest (i.e., DC to $2f_{ms2}$), to be presented in the following section.

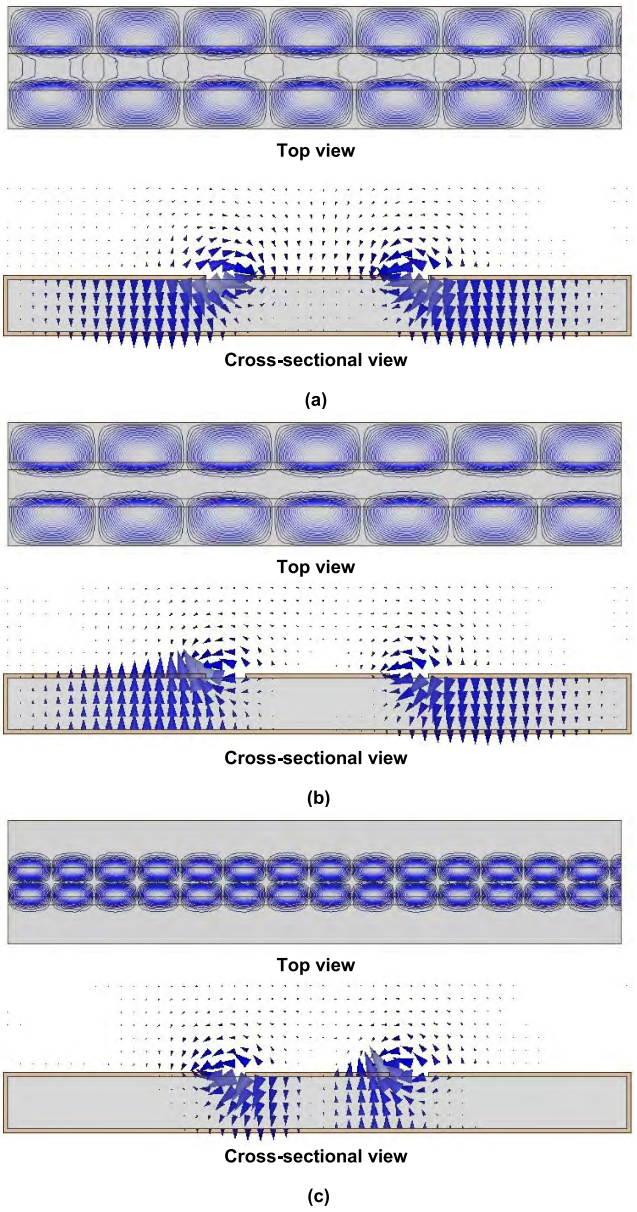

FIGURE 13. Electric field distributions for higher-order modes in MSTL. (a) Even EH_1 mode. (b) Odd EH_1 mode. (c) EH_1 mode.

VI. EXPERIMENTAL VERIFICATION

We have conducted numerical and theoretical analyses of MSTL. In this section, both MSTL I and MSTL II are implemented and characterized for an experimental verification. To facilitate the measurement and to suppress the higher-order modes, we will present a tapered microstrip-to-MSTL transition, showing properties of low loss and ultra-broad bandwidth.

A. MICROSTRIP-TO-MSTL TRANSITION

Transitions between MSTL and conventional transmission media are required for practical measurement and circuit integration. A tapered transition between microstrip line

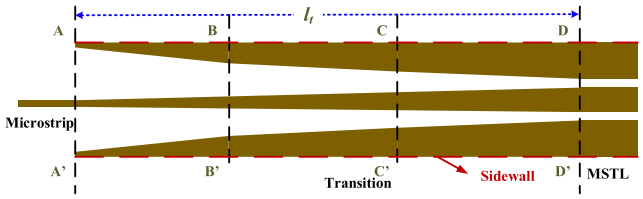

FIGURE 14. Top view of a tapered microstrip-to-MSTL transition.

and MSTL is designed, supporting a low-loss and ultra-broadband propagation. This transition is constructed by tapering the central strip inward and the side conducting planes outward symmetrically, as shown in Fig. 14. It can ensure both impedance matching and field matching between the microstrip line and MSTL [60]. More specifically, the impedance matching is mainly realized by tapering the central signal line. The field matching is assured by the central tapered line alone when frequency is in Region I (labeled in Fig. 7). In Region II and Region III, the field matching is realized by the central tapered line together with the side tapered conducting planes, able to couple a partial field energy from the central part to the side parts. The field energy can be smoothly delivered from the microstrip line on the left side of the transition to MSTL on the right side by gradually changing the physical boundary conditions, as shown in Fig. 14. The tapered transition delivering power from the microstrip to MSTL is based on the coupled-mode mechanism [11], [49]; in fact, it provides an excitation on MSTL, which is the same as the wave port in the full-wave simulations (see Fig. 1(a)).

To check the field matching of the proposed transition, we examine the electric field distributions in various cross sections of the transition labeled as A-A', B-B', C-C', and D-D' in Fig. 14. As we investigated earlier, the dominant mode of MSTL can change with frequency. Therefore, we examine the field distributions at two different frequencies, $0.5f_{ms1}$ and $2f_{ms2}$, at which the dominant mode of MSTL is the quasi-TEM mode and the quasi-TE_{10} mode of MSTL, respectively, as shown in Fig. 15. From the electric field distributions at $0.5f_{ms1}$ (see Fig. 15(a)), it is seen that the electric fields still concentrate around the central signal line, and the concentration region is changed slightly with tapering the central line. At $2f_{ms2}$ (see Fig. 15(b)), the electric fields gradually spread from the central line (see A-A') to the whole cross section (see D-D') along the transition. This phenomenon indicates that, at a low frequency (e.g., $0.5f_{ms1}$), the quasi-TEM microstrip mode of the microstrip line (see A-A' in Fig. 15(a)) is slightly adjusted to the quasi-TEM microstrip mode of MSTL (see D-D' in Fig. 15(a)). On the other hand, at a high frequency (e.g., $2f_{ms2}$), the microstrip mode of the microstrip line (see A-A' in Fig. 15(b)) is smoothly transformed to the quasi-TE_{10} waveguide mode of MSTL (see D-D' in Fig. 15(b)). In fact, the electric field distributions in A-A' are for the fixed dominant mode of the microstrip line on the left side of the transition (Fig. 14); therefore, there are slight changes at quite different frequencies. The electric field

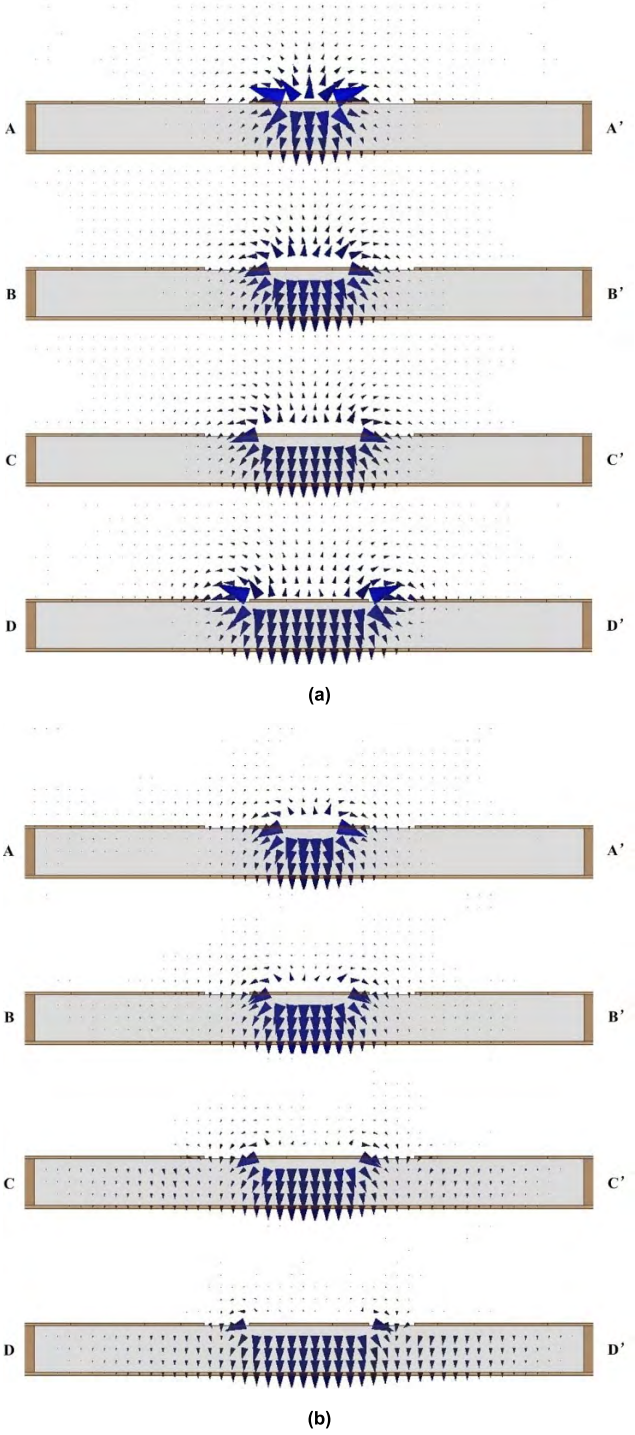

FIGURE 15. Electric field distributions in various cross sections of the transition (see Fig. 14) at (a) $0.5f_{ms1}$ and (b) $2f_{ms2}$.

distributions in D-D' are for the variable dominant mode of MSTL on the right side of the transition, and one can thus find the significantly different field distributions at different frequencies. Shown in B-B' and C-C' are the "transition" fields in the microstrip-to-MSTL transition, which are found to be analogous to those in A-A' and in D-D', respectively, resulting from the corresponding positions.

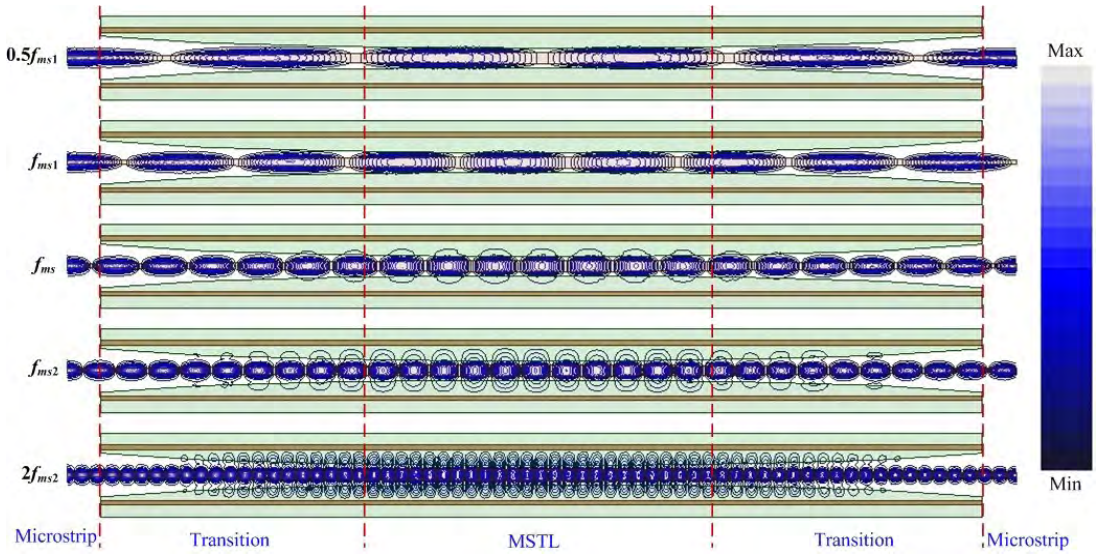

FIGURE 16. Electric field distributions along MSTL connected to two transitions at different frequencies.

Fig. 16 shows the electric field distributions along the MSTL structure connected to the transitions on two sides. Obviously, the delivery of the electric field energy along the structure at different frequencies, including $0.5f_{ms1}$, f_{ms1}, f_{ms}, f_{ms2}, and $2f_{ms2}$, is quite smooth. This further proves the capability of the proposed microstrip-to-MSTL transition in supporting well-behaved field and impedance matchings. Furthermore, at corresponding frequencies, the electric field distributions in the central MSTL of the whole structure shown in Fig. 16 are quite similar to the field distributions in a single MSTL (without transitions) listed in Table 2. This fact verifies that the microstrip-to-MSTL transition provides an excitation on MSTL, as the wave port in the full-wave simulations does (see Fig. 1(a)). Normally, a longer tapered transition could realize a smaller signal reflection, at the expense of a higher power loss [61]. This necessitates to find a trade-off between the reflection coefficient and power loss introduced by transitions. The full-wave analysis result suggests that each microstrip-to-MSTL transition could be slightly longer than three times the guide wavelength λ_g at f_{ms}, namely $l_t \geq 3\lambda_g$ where l_t denotes the transition length as labeled in Fig. 14. This maintains a low insertion loss (below 0.42 dB/λ_g) and a good return loss (better than 20 dB) over the frequency ranges of interest. Fig. 17 shows the simulated transmission and reflection responses of the single microstrip-to-MSTL transitions for both MSTL I and MSTL II. It can be observed that the single transition for MSTL I ($l_t = 21$ mm $\approx 3.8\lambda_g$) causes an insertion loss below 1.6 dB up to 60 GHz, and the single transition for MSTL II ($l_t = 3$ mm $\approx 3\lambda_g$) causes an insertion loss below 1.1 dB up to 500 GHz. Their return losses are better than 20 dB over the ultra-broad frequency ranges of interest. These results indicate that the proposed microstrip-to-MSTL transition can operate in an ultra-broad frequency range and introduce a low power loss.

In addition to the requirement for practical measurement and circuit integration, the tapered microstrip-to-MSTL transition can also effectively suppress higher-order modes in MSTL over an ultra-broad frequency range (DC to $2f_{ms2}$). As Fig. 18 shows, with the help of a single transition, the dominant mode propagates with a small loss, whereas the transmissions of the three higher-order modes (see Section V-B) in MSTL I and MSTL II are below -30 and -20 dB when frequency is up to around $2f_{ms2}$ (i.e., 60 GHz for MSTL I and 500 GHz for MSTL II). The slight difference between the suppression levels results from the different transition lengths, as described above. A close inspection of Fig. 18 shows that the transmission curves for the higher-order modes slightly rise when frequency goes below the cutoff frequencies (see Fig. 12), mainly resulting from the unwanted mode coupling. The reason for successful suppression of higher-order modes is that the transition operates in the coupled-mode approach [11], [49], and it is impossible to realize a good impedance matching and particularly a proper field matching between the dominant microstrip mode of the microstrip line and the higher-order modes in MSTL. This fact is directly observed and deduced by comparing the field distributions in microstrip line (see Fig. 2(c)) and the field distributions for higher-order modes in MSTL (see Fig. 13).

B. MSTL IMPLEMENTATION

MSTL II has been experimentally verified in [24] and [25]. Due to a high requirement for fabrication precision, a micro-fabrication process was used to implement MSTL II with micro-scale features. Detailed fabrication steps have been described in [25]. MSTL I was also fabricated to further demonstrate the practical properties of MSTL. The RT/duroid 6010LM laminate from Rogers Corporation is intentionally chosen as the MSTL substrate. Its high relative permittivity ε_r of 10.2 allows to examine the wide parameter ε_r range

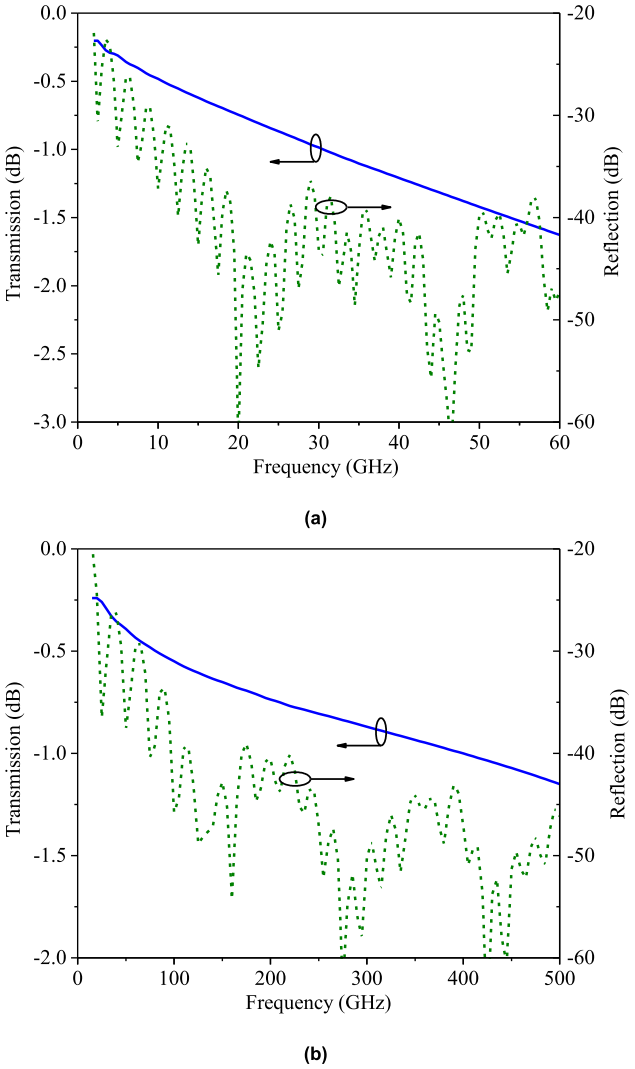

FIGURE 17. Simulated transmission and reflection responses of the single microstrip-to-MSTL transitions for (a) MSTL I and (b) MSTL II.

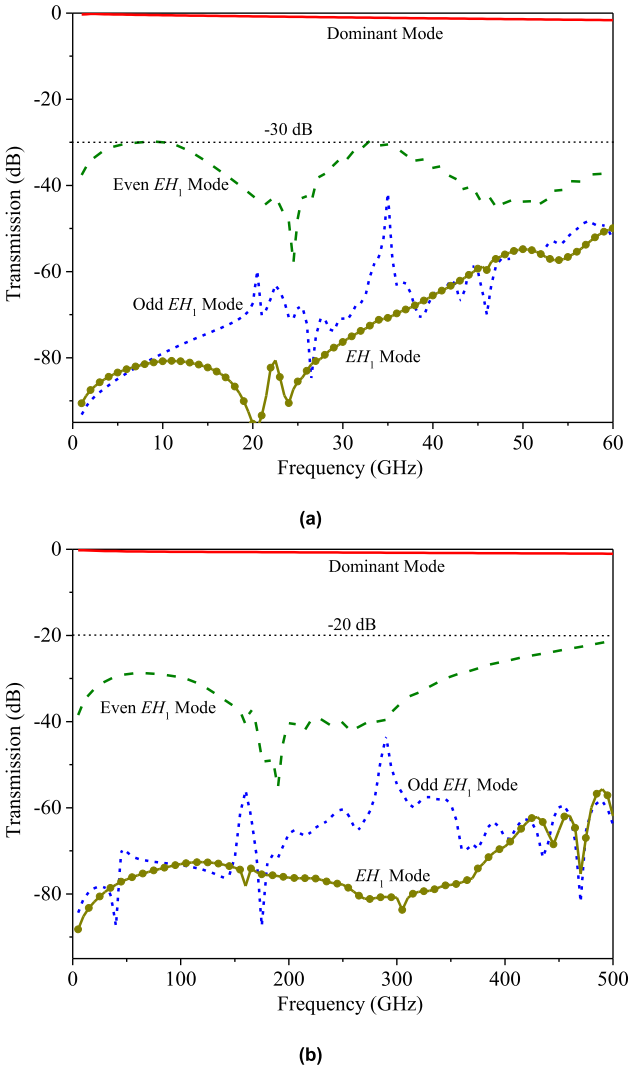

FIGURE 18. Suppression of higher-order modes in (a) MSTL I and (b) MSTL II using the single microstrip-to-MSTL transitions.

of the proposed empirical equations given in Section IV. The substrate thickness h needs to be as small as possible to weaken and even suppress the CPW mode (or slotline modes), as explained in Section II-A. The microstrip-to-MSTL transitions are used to facilitate the measurement. Given the operating frequency and the limited line width of the microstrip feeds, a dielectric substrate with a thickness of 0.254 mm is chosen rather than the commercially available thinnest counterpart with a thickness of 0.127 mm. Detailed dimensions of MSTL I are listed in Table 1. A standard printed circuit board (PCB) process technology was adopted to implement MSTL I. Note that the sidewalls of MSTL I are realized with periodically plated rectangular slots based on the SIW technology [8], [9]. Simulation results have indicated that this realization method does not cause an obvious deterioration of the MSTL performance over the frequency range of interest. The photograph of the fabricated samples of MSTL I is shown in Fig. 19. For comparison, the RWG and microstrip counterparts of MSTL I were also fabricated using the same fabrication technique. Similarly, the sidewalls of the dielectric-filled RWG are realized using the periodically plated rectangular slots; in fact, the implemented structure is an SIW. Microstrip-to-SIW transitions [9] are used to facilitate the characterization of the dielectric-filled RWG (SIW). For impedance matching, the microstrip counterpart of MSTL I is connected to two 50-Ω microstrip feed lines via two tapered lines.

C. MSTL CHARACTERIZATION

For MSTL II, the measurement was carried out on a THz station. A multiline thru-reflect-line (TRL) calibration method [62] was adopted to de-embed the effects of the test system and the transitions. A PNA-X network analyzer N5247A (Keysight Technologies) is connected to VDI transmitting and receiving frequency extenders to perform full two-port scattering parameter measurements up to 500 GHz. Measured results of MSTL II are presented in [25], revealing that MSTL II can guide an ultra-broadband (DC-500 GHz)

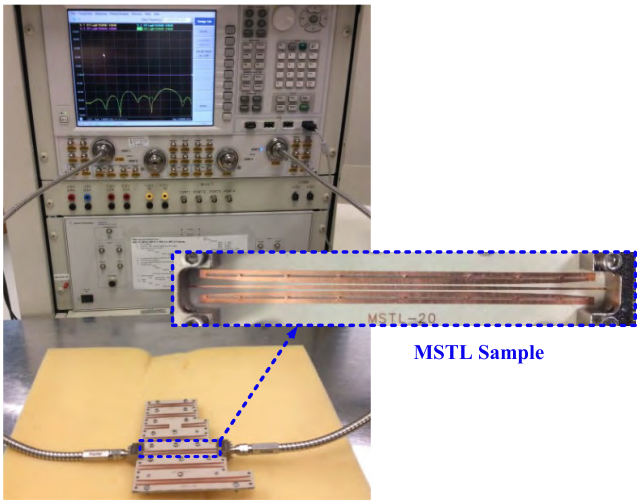

FIGURE 19. Photograph of the measurement setup and samples of MSTL I.

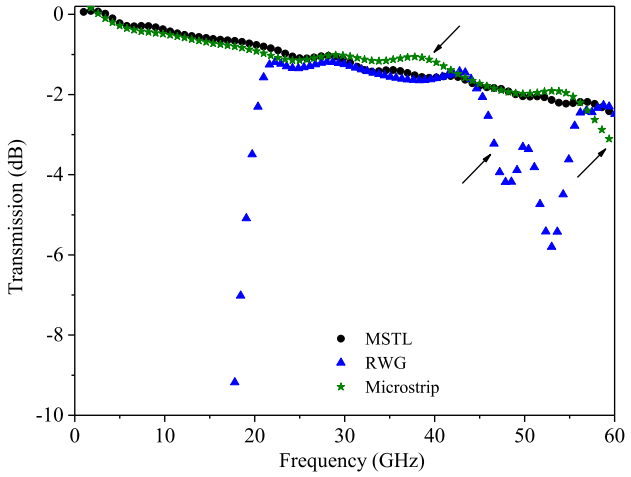

FIGURE 20. Comparison between measured transmission responses of MSTL I and its RWG and microstrip counterparts.

signal with low loss and low dispersion. For MSTL I, the network analyzer is connected to MSTL I through Southwest 1.85 mm end launch connectors. The photograph of the measurement setup is shown in Fig. 19. A measurement was carried out up to 60 GHz using the multiline TRL calibration method. The RWG and microstrip counterparts were also characterized using the same methods. Note that, the lowest measured frequency is 10 MHz, limited by the measurement setup; however, it is sufficient to demonstrate the performance near DC.

A comparison between the simulated transmission responses of MSTL I and MSTL II and their RWG and CBCPW counterparts has been carried out in Section II (see Fig. 3). Shown in Fig. 20 is the comparison between the measured transmission responses of the 20-mm-long MSTL I and its RWG and microstrip counterparts. It can be observed that MSTL I shows a smooth transmission over the whole frequency range (i.e., DC to 60 GHz). In contrast, a sharp drop at around 60 GHz in the transmission curve of the microstrip line is observed, which is due to the excitation of the first higher-order mode, EH_1 mode. Small fluctuations at around 38 GHz are also found. Consistent with the simulation results shown in Fig. 3, the RWG counterpart operates in a narrow frequency range due to the low frequency cutoff and excitation of higher-order modes at high frequencies. Through the comparison, one can find that MSTL I can operate in a wider frequency range than the microstrip and RWG counterparts. A close examination of Fig. 20 also shows that the power loss of MSTL I is comparable to the counterparts over the common frequency range of operation. In addition to the transmission response, the phase constant of MSTL I is also extracted from the measured scattering parameters [63], which is plotted in Fig. 7(a). As can be seen, the measured phase constant agrees well with the simulated one, showing a smooth phase constant curve, thus meaning a low dispersion. From these comparison results, it can be concluded that this measurement verifies the properties of MSTL.

VII. CONCLUSION

In this paper, we have investigated MSTLs comprehensively, including numerical analysis, theoretical analysis, and experimental verification. To demonstrate the applicability of the MSTL design, we have considered two MSTLs as practical examples, which operate in different frequency ranges and require different fabrication and measurement techniques. The specific phenomenon of mode selectivity in MSTLs has been verified by both the physical evidence (field distributions) and theoretical foundation (orthogonality relations). This means that a frequency-enabled mode conversion can occur in a transmission medium with a given cross section. Similar phenomenon possibly occurs in other composite transmission media. The mode selectivity has been treated rigorously by defining characteristic frequencies and then specifying several frequency regions. This will be useful for the MSTL designs with given specifications. We have also analyzed the propagation characteristics of MSTLs and have briefly discussed their higher-order modes. Higher-order modes in MSTLs can be suppressed by the proposed microstrip-to-MSTL transition, thus expanding the frequency range of operation. The comparison between the frequency characteristics of MSTLs and the conventional transmission media indicates that MSTLs can support the transmission and processing of low-loss, low-dispersion, and particularly ultra-broadband and ultra-fast signals.

Given the conditions of mode selectivity, it is possible to realize other MSTLs with frequency-enabled mode conversion among other modes, such as CPW mode and waveguide mode. Such MSTLs are promising candidates for THz chip-to-chip interconnects and other ultra-broadband applications. In addition, we could implement various MSTL-based components with high performance through benefiting from the advantages of different modes.

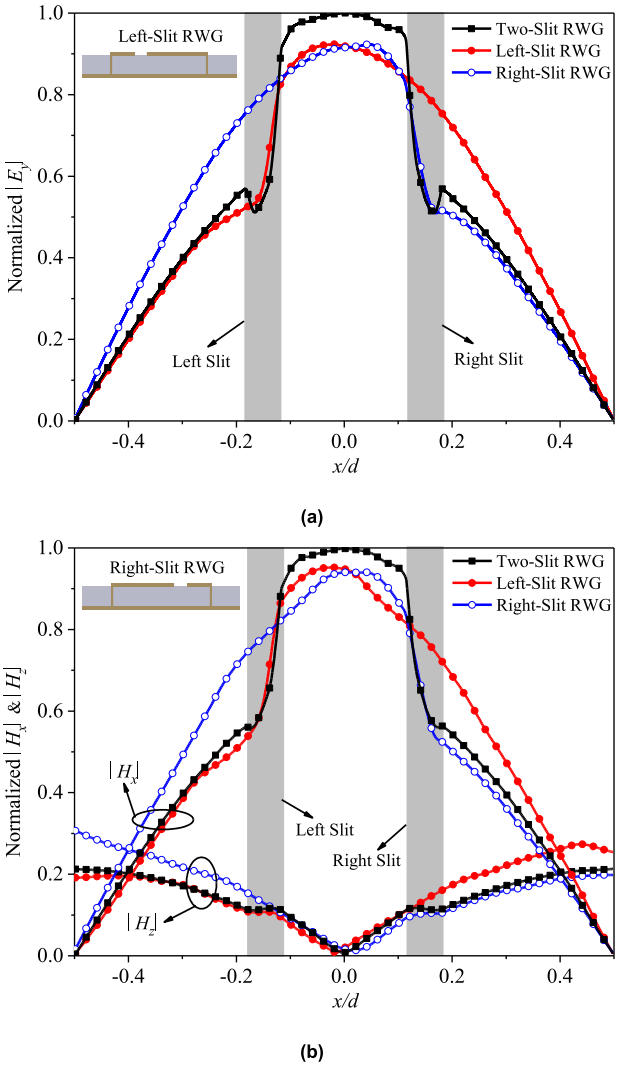

FIGURE 21. Normalized field distribution curves of the two-slit RWG, left-slit RWG, and right-slit RWG along the x-axis at 400 GHz. (a) E_y field component. (b) H_x and H_z field components.

APPENDIX

We propose a simple but rigorous method to analyze slitted RWGs in this work. MSTL II is considered as an example to introduce the method. To begin with, it is assumed that the effect of the two slits on the frequency characteristics (without considering power loss) of a two-slit RWG is a combination (linear superposition) of the effect of individual slits. The field distribution curves of the two-slit RWG and two single-slit RWGs (left-slit RWG and right-slit RWG) at 400 GHz are plotted in Fig. 21 for a visual comparison. Since the two-slit RWG in this case is used to model the individual quasi-TE_{10} waveguide mode in MSTL II, the chosen frequency point (400 GHz in this case) should be higher than the characteristic frequency f_{ms2} (defined in Section IV-B). The single-slit RWG is a dielectric-filled RWG with only one slit asymmetrically etched in the top broad wall, as shown in the insets of Fig. 21. Its dominant mode is also a quasi-TE_{10} waveguide mode. Inspection of Fig. 21 shows that the effect of both the left and right slits on the field distributions in the two-slit RWG is approximately equal to the combination (or linear superposition) of their individual effect on the left-slit RWG and right-slit RWG. This confirms the above assumption, and we can thus investigate the effect of single slit on the single-slit RWG and then simply double the effect for the two-slit RWG.

The single-slit RWG (left-slit RWG or right-slit RWG) is first analyzed in terms of phase constant and cutoff frequency. On the basis of the waveguide theory [64], empirical equations are given to calculate the phase constant β_1 and cutoff frequency f_c of the dominant quasi-TE_{10} mode of the single-slit RWG as follows:

$$\beta_1^2 = \varepsilon_r k_0^2 - \frac{k_0^2}{(k_0 + \Delta k)^2} k_{c0}^2 \tag{6}$$

$$f_c = \frac{1}{M\sqrt{\mu_0 \varepsilon_0 (\varepsilon_r + 0.34)}} \tag{7}$$

where

$$\Delta k = \frac{2\pi \cdot \Delta f}{c} = \frac{2\pi \cdot (f_c - f_{c0})}{c} \tag{8}$$

$$k_{c0} = \pi / d \tag{9}$$

$$k_0 = \frac{2\pi f}{c} \tag{10}$$

$$f_{c0} = \frac{k_{c0}}{2\pi\sqrt{\mu\varepsilon}} = \frac{1}{2d\sqrt{\mu_0 \varepsilon_0 \varepsilon_r}} \tag{11}$$

where c, μ_0, ε_0, and ε_r are the speed of light, free-space permeability, free-space permittivity, and the relative permittivity of the dielectric substrate used, respectively, and f is the operating frequency. The variable M is expressed in (3). The parameters d, h, s, and m of the single-slit RWG are labeled in the insets of Fig. 22. Fig. 22 compares the calculated and simulated cutoff frequencies f_c of the single-slit RWG versus the sidewall span d for different parameter values. Due to the limited space, the comparison is conducted for a few sets of parameter values. The value range of each parameter is expanded sufficiently. Other parameter values remain the same, as listed in Table 1. To obtain the required variable dominant mode of MSTL and to suppress undesired modes, we have defined the design region of MSTL in [26]. Within this design region, the calculation error is estimated to be less than 2%. A similar comparison for the phase constant β_1 of the single-slit RWG was also carried out, showing an acceptable calculation error of 5%.

Through comparing (6) with the equation for the phase constant of a standard RWG [19], [64], it is deduced that the term Δk in (6) and (8) is a result of the effect of the slit on the frequency characteristics of the single-slit RWG. By doubling this effect, we obtain the following empirical equations (12) and (13) to calculate the phase constant β and cutoff frequency f_{ms1} of the two-slit RWG.

$$\beta^2 = \varepsilon_r k_0^2 - \frac{k_0^2}{(k_0 + 2\Delta k)^2} k_{c0}^2 \tag{12}$$

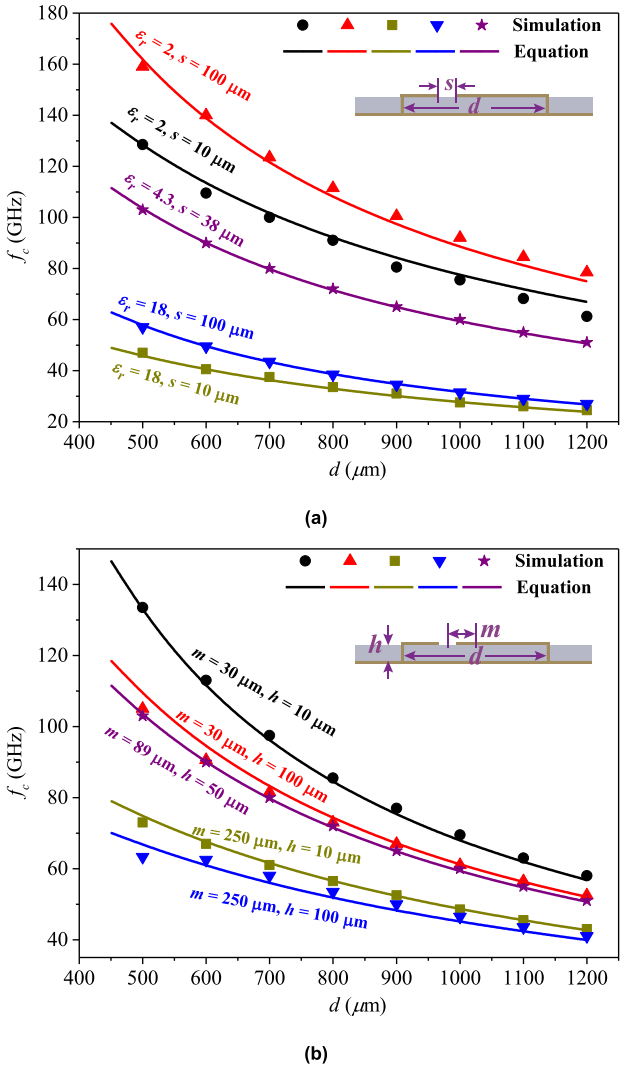

FIGURE 22. Cutoff frequency f_c of the single-slit RWG versus sidewall span d as functions of parameters: (a) ε_r and s. (b) m and h.

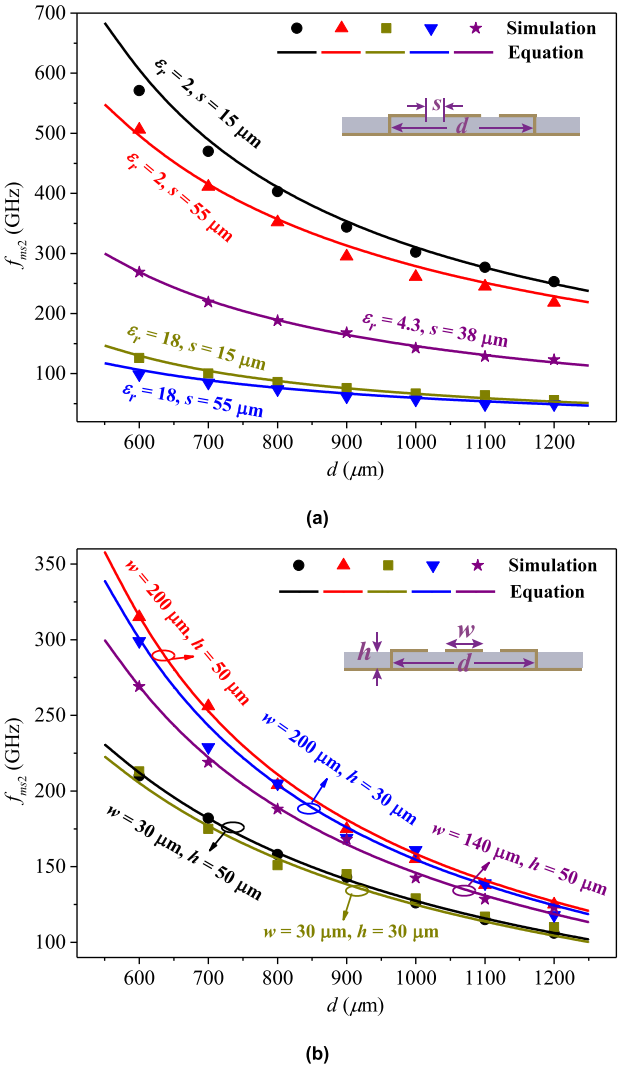

FIGURE 23. Maximum-coupling frequency f_{ms2} versus sidewall span d as functions of parameters: (a) ε_r and s. (b) w and h.

and

$$f_{ms1} = 2f_c - f_{c0} \tag{13}$$

where f_{ms1} is ultimately expressed as (2). As described in Section IV, the individual quasi-TE_{10} mode in MSTL can be modeled by the two-slit RWG, and thus (12) and (13) are also applicable to the individual quasi-TE_{10} mode in MSTL. For both MSTL I and MSTL II, the calculated phase constants and cutoff frequencies agree well with the simulated ones (see Fig. 7).

In addition to the characteristic frequency f_{ms1}, f_{ms2} is also formulated in (4). MSTL II is also considered as an example to examine the accuracy of (4). The calculated and simulated f_{ms2} for various parameter values are compared, as shown in Fig. 23. The simulation results are obtained by locating the low-frequency end of the overlapping curve of MSTL II and the individual quasi-TE_{10} mode for various parameter values. Comparison results indicate that, within the design region of MSTL defined in [26], (4) can be used to accurately predict the characteristic frequency f_{ms2} with a calculation error below 5%. Note that from the comparison results, the empirical equations given above are valid for the relative permittivity of dielectric substrate ranging from 2 to 18.

REFERENCES

[1] R. Saleh *et al.*, "System-on-chip: Reuse and integration," *Proc. IEEE*, vol. 94, no. 6, pp. 1050–1069, Jun. 2006.
[2] J. W. Holloway, L. Boglione, T. M. Hancock, and R. Han, "A fully integrated broadband sub-mmwave chip-to-chip interconnect," *IEEE Trans. Microw. Theory Techn.*, vol. 65, no. 7, pp. 2373–2386, Jul. 2017.
[3] E. Mortazy, X. Zhang, M. Chaker, and K. Wu, "Mode coupling between substrate integrated waveguide and coplanar waveguide for traveling-wave electrooptical modulator," *IEEE Trans. Microw. Theory Techn.*, vol. 59, no. 5, pp. 1258–1264, May 2011.
[4] J. Capmany and D. Novak, "Microwave photonics combines two worlds," *Nature Photon.*, vol. 1, no. 6, pp. 319–330, Apr. 2007.
[5] M. Tonouchi, "Cutting-edge terahertz technology," *Nature Photon.*, vol. 1, no. 2, pp. 97–105, 2007.
[6] G. Gallot, S. P. Jamison, R. W. McGowan, and D. Grischkowsky, "Terahertz waveguides," *J. Opt. Soc. Amer. B, Opt. Phys.*, vol. 17, no. 5, pp. 851–863, May 2000.

[7] O. Mitrofanov, R. James, F. A. Fernández, T. K. Mavrogordatos, and J. A. Harrington, "Reducing transmission losses in hollow THz waveguides," *IEEE Trans. THz Sci. Technol.*, vol. 1, no. 1, pp. 124–132, Sep. 2011.
[8] D. Deslandes and K. Wu, "Accurate modeling, wave mechanisms, and design considerations of a substrate integrated waveguide," *IEEE Trans. Microw. Theory Techn.*, vol. 54, no. 6, pp. 2516–2526, Jun. 2006.
[9] K. Wu, Y.-J. Cheng, T. Djerafi, and W. Hong, "Substrate-integrated millimeter-wave and terahertz antenna technology," *Proc. IEEE*, vol. 100, no. 7, pp. 2219–2232, Jul. 2012.
[10] S. Atakaramians, S. Afshar V., T. M. Monro, and D. Abbott, "Terahertz dielectric waveguides," *Adv. Opt. Photon.*, vol. 5, no. 2, pp. 169–215, Jun. 2013.
[11] C. Yeh and F. Shimabukuru, *The Essence of Dielectric Waveguides*. New York, NY, USA: Springer-Verlag, 2008.
[12] N. Dolatsha, C. Chen, and A. Arbabian, "Loss and dispersion limitations in mm-wave dielectric waveguides for high-speed links," *IEEE Trans. THz Sci. Technol.*, vol. 6, no. 4, pp. 637–640, Jul. 2016.
[13] C. P. Wen, "Coplanar waveguide: A surface strip transmission line suitable for nonreciprocal gyromagnetic device applications," *IEEE Trans. Microw. Theory Techn.*, vol. MTT-17, no. 12, pp. 1087–1090 Dec. 1969.
[14] R. W. Jackson, "Consideration in the use of coplanar waveguide for millimeter-wave integrated circuits," *IEEE Trans. Microw. Theory Techn.*, vol. MTT-34, no. 12, pp. 1450–1456 Dec. 1986.
[15] H.-M. Heiliger *et al.*, "Low-dispersion thin-film microstrip lines with cyclotene (benzocyclobutene) as dielectric medium," *Appl. Phys. Lett.*, vol. 70, no. 17, pp. 2233–2235, 1997.
[16] A. D. Fund *et al.*, "Metal layer losses in thin-film microstrip on LTCC," *IEEE Trans. Compon., Packag. Manuf. Technol.*, vol. 4, no. 12, pp. 1956–1962, Dec. 2014.
[17] J. Kim and H. H. Park, "A novel IC-stripline design for near-field shielding measurement of on-board metallic cans," *IEEE Trans. Electromagn. Compat.*, vol. 59, no. 2, pp. 710–716, Apr. 2017.
[18] F. David, M. Chatras, C. Dalmay, L. Lapierre, L. Carpentier, and P. Blondy, "Surface-micromachined rectangular micro-coaxial lines for sub-millimeter-wave applications," *IEEE Microw. Wireless Compon Lett.*, vol. 26, no. 10, pp. 756–758, Oct. 2016.
[19] D. M. Pozar, *Microwave Engineering*. New York, NY, USA: Wiley, 2012, ch. 3.
[20] R. Mendis and D. Grischkowsky, "THz interconnect with low-loss and low-group velocity dispersion," *IEEE Microw. Wireless Compon. Lett.*, vol. 11, no. 11, pp. 444–446, Nov. 2001.
[21] R. Mendis and D. Grischkowsky, "Undistorted guided-wave propagation of subpicosecond terahertz pulses," *Opt. Lett.*, vol. 26, no. 11, pp. 846–848, 2001.
[22] K. Wang and D. M. Mittleman, "Metal wires for terahertz wave guiding," *Nature*, vol. 432, no. 7015, pp. 376–379, 2004.
[23] K. Wang and D. M. Mittleman, "Guided propagation of terahertz pulses on metal wires," *J. Opt. Soc. Amer. B, Opt. Phys.*, vol. 22, no. 9, pp. 2001–2008, 2005.
[24] F. Fesharaki, T. Djerafi, M. Chaker, and K. Wu, "Mode-selective transmission line for DC-to-THz super-broadband operation," in *IEEE MTT-S Int. Microw. Symp. Dig.*, San Francisco, CA, USA, May 2016, pp. 1–4.
[25] F. Fesharaki, T. Djerafi, M. Chaker, and K. Wu, "Low-loss and low-dispersion transmission line over DC-to-THz spectrum," *IEEE Trans. THz Sci. Technol.*, vol. 6, no. 4, pp. 611–618, Jul. 2016.
[26] F. Fesharaki, T. Djerafi, M. Chaker, and K. Wu, "Guided-wave properties of mode-selective transmission line," *IEEE Access*, vol. 6, pp. 5379–5392, Apr. 2017.
[27] D. Deslandes and K. Wu, "Integrated microstrip and rectangular waveguide in planar form," *IEEE Microw. Wireless Compon. Lett.*, vol. 11, no. 2, pp. 68–70, Feb. 2001.
[28] R. S. Fan and R. B. Hooker, "Tapered polymer single-mode waveguides for mode transformation," *J. Lightw. Technol.*, vol. 17, no. 3, pp. 466–474, Mar. 1999.
[29] M. Thumm, "Modes and mode conversion in microwave devices," in *Generation Application High Power Microwaves*, R. A. Cairns and A. D. R. Phelps, Eds. Bristol, U.K.: IOP, 1997, pp. 121–171.
[30] J. Liu, R. Mendis, and D. M. Mittleman, "The transition from a TEM-like mode to a plasmonic mode in parallel-plate waveguides," *Appl. Phys. Lett.*, vol. 98, no. 23, p. 231113, 2011.
[31] D. S. Wang, F. Fesharaki, and K. Wu, "Physical evidence of mode conversion along mode-selective transmission line," in *IEEE MTT-S Int. Microw. Symp. Dig.*, Jun. 2017, pp. 491–494.
[32] A. Patrovsky, M. Daigle, and K. Wu, "Coupling mechanism in hybrid SIW-CPW forward couplers for millimeter-wave substrate integrated circuits," *IEEE Trans. Microw. Theory Techn.*, vol. 56, no. 11, pp. 2594–2601, Nov. 2008.
[33] J. Guo, T. Djerafi, and K. Wu, "Mode composite waveguide," *IEEE Trans. Microw. Theory Techn.*, vol. 64, no. 10, pp. 3187–3197, Oct. 2016.
[34] J. A. Deibel, M. Escarra, N. Berndsen, K. Wang, and D. M. Mittleman, "Finite-element method simulations of guided wave phenomena at terahertz frequencies," *Proc. IEEE*, vol. 95, no. 8, pp. 1624–1640, Aug. 2007.
[35] ANSYS. *HFSS Products*. Accessed: Jan. 15, 2018. [Online]. Available: http://www.ansys.com/Products/Electronics/ANSYS-HFSS
[36] R. N. Simons, *Coplanar Waveguide Circuits, Components, and Systems*. Hoboken, NJ, USA: Wiley, 2004.
[37] W. H. Haydl, "On the use of vias in conductor-backed coplanar circuits," *IEEE Trans. Microw. Theory Techn.*, vol. 50, no. 6, pp. 1571–1577, Jun. 2002.
[38] G. Leuzzi, A. Silbermann, and R. Sorrentino, "Mode propagation in laterally bounded conductor-backed coplanar waveguides," in *IEEE MTT-S Int. Microw. Symp. Dig.*, May 1983, pp. 393–395.
[39] K. Wu, Y. Xu, and R. G. Bosisio, "Theoretical and experimental analysis of channelized coplanar waveguide (CCPW) for wideband applications of integrated microwave and millimeterwave circuits," *IEEE Trans. Microw. Theory Techn.*, vol. 42, no. 9, pp. 1651–1659, Sep. 1994.
[40] A. Sain and K. L. Melde, "Impact of ground via placement in grounded coplanar waveguide interconnects," *IEEE Trans. Compon., Packag., Manuf. Technol.*, vol. 6, no. 1, pp. 136–144, Jan. 2016.
[41] C.-C. Tien, C.-K. C. Tzuang, S. T. Peng, and C.-C. Chang, "Transmission characteristics of finite-width conductor-backed coplanar waveguide," *IEEE Trans. Microw. Theory Techn.*, vol. 41, no. 9, pp. 1616–1624, Sep. 1993.
[42] Y. Shih and T. Itoh, "Analysis of conductor-backed coplanar waveguide," *Electron. Lett.*, vol. 18, no. 12, pp. 440–538, Jun. 1982.
[43] M. A. Magerko, L. Fan, and K. Chang, "A discussion on the coupling effects in conductor-backed coplanar waveguide MICs with lateral sidewalls," in *IEEE MTT-S Int. Microw. Symp. Dig.*, Jul. 1993, pp. 947–950.
[44] W. T. Lo, C.-K. C. Tzuang, S.-T. Peng, C.-C. Tien, C.-C. Chang, and J.-W. Huang, "Resonant phenomena in conductor-backed coplanar waveguides (CBCPW's)," *IEEE Trans. Microw. Theory Techn.*, vol. 41, no. 12, pp. 2099–2107, Dec. 1993.
[45] H. Shigesawa, M. Tsuji, and A. A. Oliner, "Dominant mode power leakage from printed-circuit waveguides," *Radio Sci.*, vol. 26, no. 2, pp. 559–564, Mar./Apr. 1991.
[46] D. Deslandes, "Design equations for tapered microstrip-to-substrate integrated waveguide transitions," in *IEEE MTT-S Int. Microw. Symp. Dig.*, May 2010, pp. 704–707.
[47] A. Suntives and R. Abhari, "Design and application of multimode substrate integrated waveguides in parallel multichannel signaling systems," *IEEE Trans. Microw. Theory Techn.*, vol. 57, no. 6, pp. 1563–1571, Jun. 2009.
[48] R. Garg, I. Bahl, and M. Bozzi, *Microstrip Lines and Slotlines*. Norwood, MA, USA: Artech House, 2013.
[49] A. W. Snyder, "Coupled-mode theory for optical fibers," *J. Opt. Soc. Amer.*, vol. 62, no. 11, pp. 1267–1277, 1972.
[50] J. L. G. Tornero and A. Á. Melcón, "Nonorthogonality relations between complex hybrid modes: An application for the leaky-wave analysis of laterally shielded top-open planar transmission lines," *IEEE Trans. Microw. Theory Techn.*, vol. 52, no. 3, pp. 760–767, Mar. 2004.
[51] N. K. Das, "Methods of suppression or avoidance of parallel-plate power leakage from conductor-backed transmission lines," *IEEE Trans. Microw. Theory Techn.*, vol. 44, no. 2, pp. 169–181, Feb. 1996.
[52] Y. W. Hsu and Y. C. Lin, "Modeling and characterization of slitted parallel-plate waveguide with applications for slit-based planar structures," *IEEE Trans. Microw. Theory Techn.*, vol. 65, no. 7, pp. 2228–2239, Jul. 2017.
[53] Y.-H. Chou and S.-J. Chung, "Attenuation of the parasitic modes in a shielded microstrip line by coating resistive films on the substrate," *IEEE Trans. Microw. Theory Techn.*, vol. 43, no. 7, pp. 1610–1613, Jul. 1995.
[54] P. Lampariello and A. A. Oliner, "New equivalent networks with simple closed-form expressions for open and slit-coupled E-plane tee junctions," *IEEE Trans. Microw. Theory Techn.*, vol. 41, no. 5, pp. 839–847, May 1993.
[55] H. Haus and W. P. Huang, "Coupled-mode theory," *Proc. IEEE*, vol. 79, no. 10, pp. 1505–1518, Oct. 1991.
[56] T. Sauer, *Numerical Analysis*. Upper Saddle River, NJ, USA: Pearson, 2006, pp. 230–235.

[57] Q. Lai, C. Fumeaux, W. Hong, and R. Vahldieck, "Characterization of the propagation properties of the half-mode substrate integrated waveguide," *IEEE Trans. Microw. Theory Techn.*, vol. 57, no. 8, pp. 1996–2004, Aug. 2009.
[58] D. Grischkowsky, S. Keiding, M. van Exter, and C. Fattinger, "Far-infrared time-domain spectroscopy with terahertz beams of dielectrics and semiconductors," *J. Opt. Soc. Amer. B, Opt. Phys.*, vol. 7, no. 10, pp. 2006–2015, 1990.
[59] G. F. Cheng and C. K. C. Tzuang, "A differentially excited coupled half-width microstrip leaky EH1 mode antenna," *IEEE Trans. Antennas Propag.*, vol. 61, no. 12, pp. 5885–5892, Dec. 2013.
[60] Y. Ding and K. Wu, "Substrate integrated waveguide-to-microstrip transition in multilayer substrate," *IEEE Trans. Microw. Theory Techn.*, vol. 55, no. 12, pp. 2839–2844, Dec. 2007.
[61] W. R. Klopfenstein, "A transmission line taper of improved design," *Proc. IRE*, vol. 44, no. 1, pp. 31–35, Jun. 1956.
[62] R. B. Marks, "A multiline method of network analyzer calibration," *IEEE Trans. Microw. Theory Techn.*, vol. 39, no. 7, pp. 1205–1215, Jul. 1991.
[63] W. R. Eisenstadt and Y. Eo, "S-parameter-based IC interconnect transmission line characterization," *IEEE Trans. Compon., Hybrids, Manuf. Technol.*, vol. 15, no. 4, pp. 483–490, Aug. 1992.
[64] S. J. Orfanidis, *Electromagnetic Waves and Antennas*. Piscataway, NJ, USA: Rutgers Univ. Press, 2002, ch. 9.

DESONG WANG (S'17) was born in Anhui, China, in 1988. He received the B.Sc. degree in electronic information engineering from Anhui University, Hefei, China, in 2010, and the M.Sc. degree in electronic engineering from the Nanjing University of Science and Technology, Nanjing, China, in 2013. He is currently pursuing the Ph.D. degree in electrical engineering with the École Polytechnique of Montréal, Montréal, QC, Canada.

He was an Exchange Student with Chang Gung University, Taoyuan, Taiwan, China, from 2012 to 2013, where he was involved in the development of 60-GHz passive components and systems based on a low-temperature cofired ceramic technology. He was a Research Assistant with the City University of Hong Kong, Hong Kong, from 2013 to 2016, where he was involved in the research of millimeter-wave and terahertz frequency-selective surfaces. His current research interests include microwave, mm-wave, and THz broadband transmission lines and applications.

FAEZEH FESHARAKI received the B.Sc. degree in electrical and computer engineering from the Isfahan University of Technology, Iran, in 2008, the M.A.Sc. and Ph.D. degrees in electro-optic and microwave engineering from the École Polytechnique of Montréal, Canada, in 2012 and 2016, respectively.

She was a Post-Doctoral Research Fellow with the Optical Systems and Technology Laboratory and also with the Nanoplasmonic Laboratory, University of Victoria, Canada. She is currently involved in cutting-edge integrated circuit technology with Microsemi (semiconductor and system solutions). Her research interests include dc to terahertz (THz) substrate integrated circuits and printed circuit boards, THz photonic, THz nanoplasmonic antenna and transceiver, and advanced computer aided design and modeling techniques. She was a recipient of NSERC and FRQNT Fellowships.

KE WU (M'87–SM'92–F'01) received the B.Sc. degree (Hons.) in radio engineering from the Nanjing Institute of Technology (now Southeast University), China, in 1982, the D.E.A. degree (Hons.) in optics, optoelectronics, and microwave engineering from the Institut National Polytechnique de Grenoble, France, in 1984, and the Ph.D. degree (Hons.) in optics, optoelectronics, and microwave engineering from the University of Grenoble, France, in 1987.

He was the Founding Director of the Center for Radiofrequency Electronics Research of Quebec (Regroupement stratégique of FRQNT) and the Tier-I Canada Research Chair in RF and millimeter-wave engineering. He has held guest, visiting, and honorary professorships with many universities around the world. He has been the Director of the Poly-Grames Research Center, École Polytechnique de Montréal. He is currently a Professor of electrical engineering, and the NSERC-Huawei Industrial Research Chair in future wireless technologies with the Polytechnique Montréal (University of Montreal), QC, Canada. He is also with the School of Information Science and Engineering, Ningbo University, on leave from his home institution, leading a special 5G and future wireless research program there. He has authored or co-authored over 1200 referred papers and a number of books/book chapters. He has filed over 50 patents. His current research interests involve substrate integrated circuits, antenna arrays, field theory and joint field/circuit modeling, ultra-fast interconnects, wireless power transmission and harvesting, and MHz-through-THz transceivers and sensors for wireless systems, and biomedical applications. He is also interested in the modeling and design of microwave and terahertz photonic circuits and systems.

Dr. Wu is a fellow of the Canadian Academy of Engineering and the Royal Society of Canada (The Canadian Academy of the Sciences and Humanities). He is a member of the Electromagnetics Academy, Sigma Xi, URSI, and the IEEE-Eta Kappa Nu. He was an elected IEEE MTT-S Administrative Committee (AdCom) Member from 2006 to 2015. He is the inaugural representative of North America as a Member of the European Microwave Association General Assembly. He was a recipient of many awards and prizes, including the first IEEE MTT-S Outstanding Young Engineer Award, the 2004 Fessenden Medal of the IEEE Canada, the 2009 Thomas W. Eadie Medal of the Royal Society of Canada, the Queen Elizabeth II Diamond Jubilee Medal in 2013, the 2013 FCCP Education Foundation Award of Merit, the 2014 IEEE MTT-S Microwave Application Award, the 2014 Marie-Victorin Prize (Prix du Quebec-the highest distinction of Québec in the natural sciences and engineering), the 2015 Prix d'Excellence en Recherche et Innovation of Polytechnique Montréal, and the 2015 IEEE Montreal Section Gold Medal of Achievement. He has held key positions in and has served on various panels and international committees, including the chair of Technical Program Committees, International Steering Committees, and international conferences/symposia. In particular, he was the General Chair of the 2012 IEEE Microwave Theory and Techniques (IEEE MTT-S) International Microwave Symposium. He was the Chair of the joint IEEE chapters of MTT-S/AP-S/LEOS, Montreal, QC, Canada. He has served as the Chair of the IEEE MTT-S Transnational Committee, Member and Geographic Activities Committee, and Technical Coordinating Committee, among many other AdCom functions. He is currently the Chair of the newly restructured IEEE MTT-S Montreal Chapter. He was the 2016 IEEE MTT-S President. He has served on the editorial/review boards of many technical journals, transactions, proceedings, letters and scientific encyclopedia, including as an editor or a guest editor. He was an IEEE MTT-S Distinguished Microwave Lecturer from 2009 to 2011.